UCLouvain

AGRO LOUVAIN

Faculty of bioscience engineering

Soil moisture mapping using a drone-borne Ground Penetrating Radar

A tool for precision agriculture and soil hydrodynamic modelling

Author	Margot Dehem
Supervisor	Sébastien Lambot (SST/ELI/ELIE)
Readers	François Jonard (SST/ELI/ELIE)
	Bas van Wesemael (SST/ELI/ELIC)
Academic Year	2019 - 2020

Thesis presented in partial fulfilment of the requirements for the degree of Master in environmental bioengineering

Acknowledgements

I'd like to thank firstly Sébastien Lambot for offering me the opportunity to work on this subject and for the time spent, ensuring the progress and accomplishment of my thesis despite the outbreak of Covid19 and the consequent difficulties.

I'd like to thank Kaijun Wu for all the precious help she gave me, tutoring me for Latex, Python, Matlab, for all my questions concerning the theory of GPR and inversion, and a lot more.

I'd also like to thank Elisabeth Peremans for being a great partner. Working together was a pleasure and it was always helpful to solve our difficulties together.

I would evidently also like to thank the two readers of my thesis, Bas van Wesemael and François Jonard for the time it will take them to read and assess this paper.

Finally I'd like to thank my family who has played the essential part of proof reading and supporting me during the entire process.

List of abbreviations

ABAS Aircraft-based augmentation system

AW Air wave

AWM Agricultural water management

CMP Common midpoint

CNSW Carte numérique des sols de Wallonie

CW Continuous wave

DEM Digital elevation model

dGNSS Differential global navigation satellite system

dGPS Differential global positioning system

EGNOS European geostationary navigation overlay service

EMI Electromagnetic induction

ERT Electrical resistivity tomography

ET Evapotranspiration

FAE Field application efficiency

FAO Food and agriculture organisation

FO Fixed offset

GBAS Ground-based augmentation system

GCP Ground control points

GDOP Geometric dilution of precision

GIS Geographical information systems

GNSS Global navigation satellite system

GPR Ground penetrating radar

GPS Global positioning system

GW Ground wave

IoT Internet of things

LPWAN Low-power wide-area network

LUT Look-up table

NDVI Normalized difference vegetation index

NTRIP Networked Transport of RTCM via Internet Protocol

PCA Principal components analysis

PEC Perfect electrical conductor

PPK Post processing kinematics

PRD Partial root-zone drying

RDI Regulated deficit irrigation

RTK Real time kinematics

SAR Single aperture radar

SBAS Satellite-based augmentation system

SFCW Stepped-frequency continuous-wave

SWC Soil water content

TEM Transverse electromagnetic

TDR Time domain reflectometry

UAV Unmanned aerial vehicle

VNA Vector network analyser

VRI Variable rate irrigation

VRT Variable rate technologies

VSWC Volumetric soil water content

WAAS Wide area augmentation system

WARR Wide angle reflection and refraction

WSN Wireless sensor network

WUE Water use efficiency

Contents

Chapter 1

Introduction

1.1 Context

In order to reach towards the United Nation's sustainable development goals, and more specifically the ones about food sovereignty and climate change mitigation, a significant effort needs to be made within the sector of agriculture. Indeed, this sector on it's own is responsible for 24% of greenhouse gas emissions [1] and 70% of freshwater withdrawal [2]. Conventional farming and its derivatives of excessive use of chemicals and water resources has also led to negative impacts on the environment such as soil erosion and degradation as well as pollution of groundwater and of the atmosphere.

The need for agricultural production to sustainably develop itself is rather urgent given the projected increase of global population for the coming decades. The aim is to be more productive and less wasteful, using sustainable agricultural practices to preserve healthy soils, to cope with scarcity of freshwater, to prevent organic and artificial fertilizers from polluting the environment, and more. Furthermore, the sustainability of agriculture and food systems is threatened by expected changes in temperature, precipitation and pests [3]. It is therefore crucial to invest in research and development of new technologies such as soil moisture monitoring for sustainable agriculture.

While global soil moisture has slightly increased during the second half of the twentieth century simultaneously with an increase in temperature and in precipitation [4], the trend is reversed since the beginning of the twenty-first century, the rise of ET having surpassed the precipitation rise [5] [6] [7]. On top of the drying trend, there is also a rising spatial and temporal variability in ET, precipitation, evaporation and atmospheric water-vapour content which are causing variability in soil moisture and the intensification of the entire hydrologic cycle [5]

Beyond being essential to agricultural production, soil moisture also impacts land carbon uptake [8]. Indeed, approximately 25% of anthropogenic CO_2 emissions are absorbed by the terrestrial biosphere. So, when primary production is limited by water stress, the carbon storage is negatively affected and when soil-moisture variability increases, the land carbon sink is reduced

[9].

1.2 Objectives

The general purpose of soil moisture mapping using a drone-borne Ground Penetrating Radar is monitoring soil water content of agricultural fields to support precision agriculture and achieve a better understanding of the field's hydrology. Indeed, in precision agriculture, it is opportune to acquire high volumes of information that may be utilized to advise decision making, leading to better yields, conservation of soils, and reduction of freshwater waste. And with this spatially and temporally dense grid of data concerning soil water status, a better understanding of hydrological processes at the field scale is achievable.

The specific objectives of this master's thesis are to use a drone-borne GPR with a dipole antenna on an agricultural field in Wallonia in order to produce high resolution maps and study the spatial distribution as well as the dynamics of soil water content.

1.3 Methodology and outline

After this brief introduction, chapter two gives a review of agricultural water management, precision agriculture and soil water content monitoring, chapter three covers the electromagnetic principles, survey methods, antennas, and the inversion using a ground penetrating radar. Chapter four goes through positioning technologies. In chapter five, soil moisture maps are generated from GPR data acquired on an agricultural wheat field in Gembloux. And finally, chapter 6 serves as conclusion for this paper. This master's thesis is indeed quite bibliographical on account of the Covid19 lockdown which postponed field work and made laboratories unavailable.

Chapter 2

State of the art

2.1 Agricultural water management

At the core of agriculture comes water, it is without a doubt the most precious resource necessary for food production. This input needs to be precisely measured, because both shortage and excess impact severely yield and quality of the production. While basin scale agricultural water management (AWM) aims at adjusting the budget for water conservation and the advantages of future water availability, field scale AWM targets the producer's profit through efficient irrigation for example [10]. This thesis focuses on the field scale. Consequently, two water management operations are specified at the field scale : drainage and irrigation.

Despite the important water stress in some areas, drainage becomes a key operation for agricultural water management after important precipitations or in a zone that is inclined to flooding. Artificial drainage is the removal of excess water from above or below the soil surface, supporting natural drainage when it is insufficient. After a heavy rainfall, or in flooded zones, it is crucial that a saturated soil be drained before irreversible damage is done to plant growth due to the anaerobic conditions in the root zone. Setting aside risks from the rise of the water table is key to optimise production for most crops, even though there are exceptions, such as rice, which support anaerobic conditions well. Artificial drainage is also useful to facilitate the use of machinery on water logged terrains [11].

With non satisfying or inconsistent rainfall, it is irrigation that takes on a key role in food production systems. In 2010, 20% of total arable crop land was irrigated and all this irrigated surface was responsible for 40% of global harvest [12] [2]. Meanwhile, freshwater is only 2,5% of total water present on earth and this freshwater is greatly stored in glaciers and deep groundwater, making it difficult to access [13]. Given the increase in total irrigated land surface over time, the fact that freshwater is a key input for crop production, and the growing demand for water in all human activities, a good management of this scarce resource is essential to sustain our future needs [2]. In order to cope with this increasing pressure, water use efficiency is imperatively urged to increase and solutions such as the use of treated wastewater for irrigation are encouraged.

2.1.1 Irrigation systems

Among the different irrigation systems that are available, the choice of one will depend on numerous factors such as crop type, the quality of the water used, soil properties, the topography of the irrigated surface and compatibility with the management techniques, aiming at a high efficiency and low labour and financial requirements [14].

2.1.1.1 Surface irrigation

Also known as gravity flow distribution, this method of irrigation uses a free surface and overland flow of irrigation water to supply crops. This method is thousands of years old and originated in the flood plains around rivers where farmers used canals and small channels to allocate river water to their crops. Today it is stays the most popular irrigation method, still accounting for 94% of global irrigation in the world in the nineties [15]. The design of surface irrigation has evolved due to pumps especially which permit to extend this practice outside of flood plains.

The advantage of this technique is economical and practical. When the fields topography permits it, surface irrigation might be the cheapest and easiest design to water crops. However, as hinted previously, there is a constraint on the field slope, which needs to be small enough to limit an uneven distribution of water infiltration in the field. If this isn't the case, the farmer will be obligated to level or grade the field, inducing elevated construction costs to ensure the steady gravity distribution [14] [15].

2.1.1.2 Sprinkler irrigation

Sprinkler irrigation is a pressurized application of water through a nozzle. The water is sprayed onto the crops, resembling a natural rainfall [16]. Fields with an elevated slope that are unfit for surface irrigation might be well adapted to this form of irrigation. Pipe sizes can be designed to adapt to different elevations in order to reach uniformity in infiltrated water across slopes. However, a disadvantage of this system is the possible evaporation and drift of droplets before they reach the soil surface, which is especially a problem in arid or windy areas. Other disadvantages are the necessary energy for pressurization and the harm caused by the quality of the water on the pipe system due to sedimentation of solutes. The center pivot is a popular design of a sprinkler irrigation system [15] [14].

2.1.1.3 Micro irrigation

Also known as drip irrigation or trickle irrigation, this method applies droplets of water directly to the root zone of a plant with a low pressure and a low volume discharge. The application can be either above or below the soil surface. Used in arid zones because of its efficiency, it spares a lot of water by minimizing evaporation and applying water locally. It is an irrigation method that targets the crop, leaving the soil around it dry and inhospitable to weeds

that would compete for nutrients and moisture. The disadvantage of this system is it's high capital costs, making it profitable mainly for high value crops [15] [14] [17].

2.1.1.4 Subirrigation

In subirrigation, relatively large amounts of applied water percolate through the ground in order to obtain a controlled water table. Then, through an upward capillary flow from this groundwater table the root zone is supplied with enough water content for plant growth [15] [14]. This method is used in regions where the water table is shallow.

2.1.2 Sustainability of agricultural water management

A development of agricultural water management that satisfies present needs without compromising future generations' needs can be carried out by the search for better water use efficiency, use of clean energy and restoration and preservation of soils.

Water use efficiency (WUE) can be defined economically as the monetary return obtained from irrigation compared to the investment made for the input of water. However, costs and benefits linked to irrigated crops are not all economically well represented, especially long term costs and benefits such as the risk for soil degradation [17].

To have a more physical indication on the use of water, field application efficiency (FAE) measures directly the fraction of consumed water to the volume of total applied water (eq. 2.1). The water consumed by the crop can be approximated as the transpired water since only about 1% is absorbed and included in the vegetative biomass while the remaining 99% is transpired (eq. 2.2). FAE can thus be quantified as crop growth relative to total water applied, given that transpiration and CO_2 uptake happen simultaneously through stomatal opening, and that photosynthesis proportionally happens with CO_2 uptake. FAE is also called crop water use efficiency, it measures the response of the crop to irrigation. Field application efficiency is reduced by surface run-off, deep percolation below the root zone and evaporation of applied water directly from the soil surface or from the leaves. The chosen method of irrigation may strongly limit losses through evaporation [17].

$$\text{FAE} = \frac{\text{consumed water}}{\text{total applied water}} = \frac{\text{total applied water} - \text{wasted water}}{\text{total applied water}} \tag{2.1}$$

$$\text{FAE} \approx \frac{\text{transpired water}}{\text{total applied water}} \tag{2.2}$$

Improving FAE can be achieved by conservation of water and by increase of crop growth [18]. It is important because it implies a considerate sparing of freshwater resources and the prevention of soil degradation due to over-irrigation [19]. The harmful effects of poor water management on soil quality causing a decline of crop productivity impact not only the environment, but also

the economy and social well-being.

Sustainability of water management also includes several innovations and practices such as the use of green energy for irrigation purposes. Examples of solar powered irrigation systems for efficient allocation of water have lead to more sustainable systems. Sustainability is also supported by enhancing long-term soil health and consequently crop productivity.

In order to encourage sustainability of AWM and efficient water use, several agricultural practices are presented in the next section.

2.1.3 Agricultural practices for efficient water use

The promotion of certain management practices can increase crop water use efficiency while minimizing negative environmental impacts [10]. Some examples of these agricultural practices are given below.

- Choice of an appropriate irrigation method to reduce evaporation. Possibly requiring land levelling, terracing or other arrangements [18] [20].
- Choice of crops that are well adapted to the local soil and climate.
- Optimization of growing conditions with a wise timing for the successive operations of tillage, planting, fertilizing, pest control and harvesting [17].
- Use of rainwater and development of engineering facilities to retain, gather, store and transport it [20].
- The introduction of cover crops for enhancement of soil structure and water retention properties.
- Development of carbon pools by fertilizing or fertigation : There is an interaction between water use and nutrient availability, and with increased soil nutrients not only crop yields are better but also WUE/FAE by increasing the soil's water holding capacity and by enhancing root volume [20].
- Conservation tillage (no-till or minimal till) to conserve soil moisture and improve soil properties, aggregate stability. Avoiding harmful long term consequences such as reduction of soil porosity and compaction of the topsoil can be done by combining conservation tillage with subsoiling once every couple of years in a rotational pattern to optimise soil properties on the long run [20].
- Mulching. It is the application of a material over the surface of the soil as a covering strategy to reduce evaporation from the soil, to prevent weed growth, to keep the soil temperature fresh and amend nutrients to the soil (if mulch is organic and decomposing).

- Regulated deficit irrigation (RDI). It is the practice of irrigating below the crop water requirements resulting in a higher water use efficiency. Three techniques of RDI are presented.

    1. Applying RDI at specific non-critical stages of crop development, based on the fact that the response to water stress is variant at different stages of development. It can be used to stimulate flowering or budding for example [20].
    2. Partial root zone drying (PRD) alternates irrigation between two halves of the root system (see fig. 2.1). The benefits of this technique rely on the hypotheses that the dry half of the roots might respond to water stress by sending a signal to the shoot and might reduce substantially water loss without affecting photosynthesis drastically. With PRD, plants can proceed to osmotic adjustments by accumulating substances. PRD stimulates protective processes [20].
    3. Supplemental irrigation which consists in irrigating when a shortfall of precipitation occurs. This requires knowledge on soil water content and a reliable weather forecast [20].

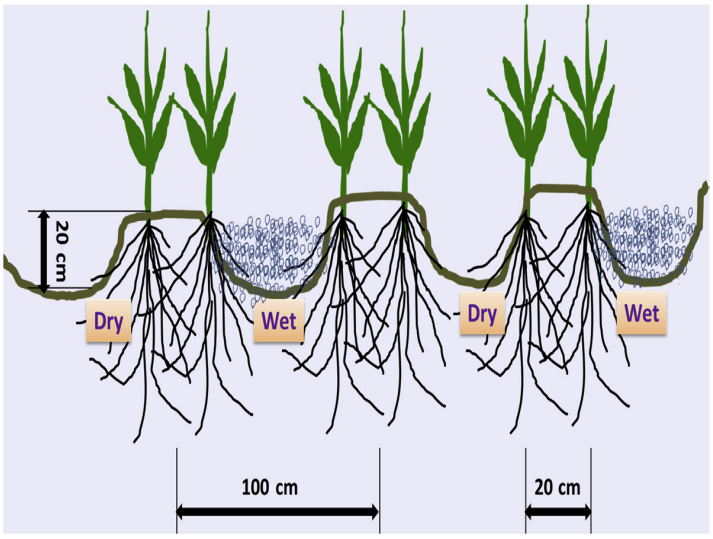

Figure 2.1: Partial root zone drying [20].

- Chemical regulation is a technique to reproduce the plant's response to water deficiency. Plant hormones such as abscisic acid signal soil drying and consequently reduce transpiration by stomatal closure or leaf rolling. Thus a study shows that amending the soil with abscisic acid and β-aminobutyric acid can decrease or slow water use and increase WUE. Another example of chemical regulation is the use of a plant growth regulator, such as uniconazole, which boosts root growth and hence access to soil water as well [20]. More research needs to be done to inventorise all side effects of the use of these chemicals.

Generally, the development of instrumentation and techniques for the measurement and quantity control of distributed irrigation water is useful for sustainable agricultural water management [20].

2.1.4 Challenges and opportunities in water efficient agriculture

Finally, a choice needs to be made between optimising crop yields and optimising water use efficiency, considering the effects of conversion of more land for extensive farming and the effect of salt accumulation [21]. This accumulation happens when irrigation water contains solutes and when farmers are supplying minimal quantity of water to crops, preventing salts to flush to deeper layers [22].

While climate change will strengthen the need for good agricultural water management given the change in precipitation patterns and intensities, global population increase will strengthen the need for more agricultural production. This increase may come from better crop yields, from additional agricultural lands, from the development of urban agriculture, from better water use efficiency. Furthermore, a better understanding of crop response to drought is necessary regarding frequency, the degree and the duration of the dry season [23]. The expanding requirement for water in all human activities proportional to economic growth drives a competition between different sectors and influences agriculture to restrain its water use.

2.2 Precision agriculture

Precision agriculture is a low-input, high-efficiency, sustainable agriculture which comes as a step in the evolution of agriculture through time. It is the current information age which permits us to integrate the numerous technological advances to agriculture, after the industrial age which brought mechanisation and synthesized fertilizers and after the technology age which was the time of innovation with genetic engineering and automation [24].

Made possible by the rapid development of information technologies across all fields and subjects, precision agriculture uses a management strategy of integrating an elevated amount of data in a wide range of technologies and practices to make informed agricultural decisions in order to boost productivity while reducing production costs and environmental impacts [25].

The typical procedure comprises three steps [25] [24] :

1. Acquisition of comprehensive data about crop production and soil properties as well as variability in space and time.

2. Analysis and interpretation of multi-source data.

3. Implementing of a management strategy based on the collected information, using the appropriate choice of spatial and temporal scale.

The benefits of precision agriculture are economic and environmental gains through a better efficiency and less consumption of inputs. Specifically, this means profitability for farmers due to higher yields and environmental benefits by the saving of water resources and the impediment

of organic fertilizers leaking to the environment.

However, it is not so obvious that revenue from the additional yield due to precision agriculture counterbalances the costs relative to the implementation of these technologies. Larger farms may have a better opportunity at viable precision agriculture than small ones [24]. Furthermore, the technologies useful for precision agriculture are only emerging and they might not be profitable yet in their early stages of adoption, but research and development on them will certainly improve their accuracy, spatial resolution and costs of operation [25].

2.2.1 Variable Rate Technologies

The spatial variability of soil properties has been targeted as one of the most important hindrances to maximisation of crop productivity [26]. Therefore, one of the main principles of precision agriculture is to manage the variability in a field. To deal with the heterogeneity on a given field, VRT, or variable rate technologies are used to manage within-field variability and permit a targeted application of inputs. The consequence of this new-found precision in input distribution is an improvement in production efficiency.

The idea of VRT is to implement a site-specific management, dividing the field into smaller zones and using observations on a finer spatial (and temporal) scale instead of using the average field conditions [25]. These units, called management zones, aiming to have homogeneous soil and/or crop properties, or at least little variability, are delineated by different techniques of clustering. Methods such as principal component analysis (PCA) are useful to create new independent variables and chose the most important principal components to delineate coherent management zones when many variables impact crop yields. Other methods such as k-means and fuzzy k-means can also be useful. Delineating robust zones may use a single or multiple soil and/or crop characteristics such as soil water content, soil apparent electrical conductivity, soil texture, terrain elevation,... [27]

A reasonable number of management zones, given the total size of the field, needs to be determined, depending on the machinery's functioning. Excessively small zones are ineffective because it isn't possible to differentially manage them [24]. The shape of the management zones can also be a technical constraint given by some apparatus. Therefore, a study proposes a method to delineate rectangular management zones based on soil properties to facilitate operation of machinery [26].

These management techniques are commonly separated between map based and sensor based techniques [24] [27]. The map based VRT technologies use GPS, remote sensing, and soil sampling to create a grid of data and interpolate it with geostatistical methods. The sensor based technologies are rather expensive, but they provide real time information and don't necessarily need GPS positioning because of the in-situ placement of the sensors. They aren't as common as map based technologies because of the aforementioned high cost as well as the

usual inaccuracy of most sensors [24].

The use of variable rate technologies is on one hand driven by an increase of within-field variability through time. Indeed, farm and field sizes have increased, and with that comes an obvious rise in heterogeneity within the field. On the other hand, VRT technologies are made possible by the technological advances and innovation throughout different sectors (e.g. : GPS, GIS, remote sensing, microelectronics, sensors, telecommunications,...) [24].

2.2.2 Geographical information

In precision agriculture it is often necessary to georeference the collected data. Information from different sources can be used together and associated for a better understanding of spatial variability and for sub-field management.

GIS, or geographical information systems, is a mapping software used to digitalize, analyse, store, produce and display georeferenced data [25]. GIS is useful to improve data management, data integration by combining consistent multiple sources, data accessibility by standardization of formats, scenario simulation and quality and response time. GIS can for example be used to create yield potential maps to support information based decision making by converting these yield maps into differential management plans [24].

GPS or global positioning system is an American tool using a constellation of satellites for geographical data acquisition. Simultaneous reception of minimum four satellite transmissions are required to retrieve an accurate reading of latitude and longitude. In order to retrieve coordinates or navigational guidance with a 15m accuracy more or less, GPS technology functions with distance measurements, triangulation and some corrections [25].

See chapter 4 for a more in-detail review of positioning technologies.

2.2.3 Variable Rate Irrigation

Variable rate irrigation (VRI) is a management strategy of allocating different amounts of irrigation water to different management zones of agricultural plots. The depth of water application varies to take into account soil type variability, crops, and other conditions [28].

A main method of conducting VRI consists of producing speed control maps for the central pivot irrigation system. The result will be that the central pivot will increase its speed where less water requirements are exhibited and slow down where irrigation needs are higher. The intelligent decision making system may use data from different sources such as remote sensing of the normalized difference vegetation index (NDVI) and canopy temperature by infrared remote sensing [28].

Figure 2.2 shows the structure of a decision support system for variable rate irrigation based on UAV multispectral remote sensing [29]. The figure shows the four steps and their different functions :

1. UAV campaign and collection of data : Acquisition of multispectral images and meteorological data.

2. Data processing : Establishment of crop evapotranspiration model, crop water stress index and precipitation.

3. Fuzzy system : Using the three inputs mentioned above, control information is produced for the regulation of the solenoid valve for each segment of the center pivot's impact area.

4. Control map for the variable speed of a center pivot irrigation device and the varying solenoid valve openings.

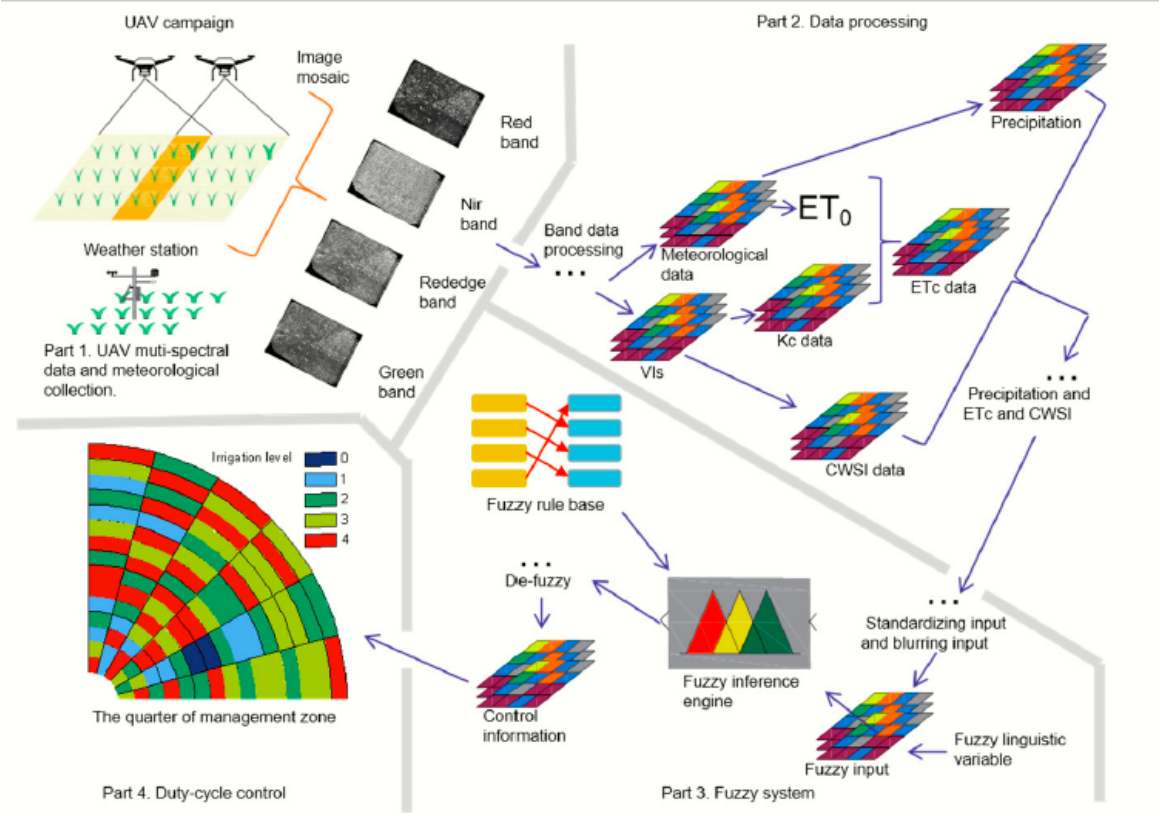

Figure 2.2: Structure of the intelligent irrigation system (extracted from [29]).

Irrigation scheduling can also rely on a wireless sensor network (WSN) to monitor soil water content and meteorological data [29]. The search of automated solutions for VRI has for example led to the creation of WaterBee, an EU-funded project that developed a prototype of soil-moisture modelling with a web based wireless sensor network aiming at water use efficiency optimisation in smart irrigation [30].

2.3 Soil water content monitoring

In order to provide information on crop water requirements, monitoring of soil water content (SWC) can be a tool [25]. There are many different methods to measure soil water content. Below, the gravimetric method, the neutron probe, and several electromagnetic methods are exposed. For effective irrigation, monitoring the spatial variability of soil water content needs a sub-metre resolution, especially in arid regions or with high value crops (ex: vineyards) [31] [32].

2.3.1 Gravimetric and volumetric soil water content

The gravimetric soil water content can easily be found by a simple oven drying technique. The difference in mass between the soil sample before and after 48 hours at 105°C is used as the mass of water in the soil sample. This mass of water is converted in a volume in order to retrieve volumetric soil water content (see equations 2.3 and 2.4 below). This method is direct and highly precise but the scale is quite narrow and it is destructive.

Gravimetric water content θ_w (g/g) :

$$\theta_w = \frac{M_t - M_s}{M_t} \tag{2.3}$$

Volumetric water content θ_v (cm^3/cm^3) :

$$\theta_v = \frac{(M_t - M_s)/\rho_w}{V_t} \tag{2.4}$$

With,
M_t = Total mass of the soil sample (g)
M_s = Mass of the dry soil sample (g)
ρ_w = Volumetric mass density of water (g/cm^3)
V_t = Volume of soil sample (cm^3)

2.3.2 Neutron probe

The neutron probe is an indirect method to quantify water content. It emits fast neutrons in the soil, and since neutrons are deflected by hydrogen which is most common in water, the detected and counted slow neutrons give an estimation of soil water content. The probe can be placed on the soil surface or in a borehole that serves as an access tube to survey deeper. The neutron scattering covers a spherical domain, and the sampling volume will depend on soil moisture, and thus influence depth resolution. Near the soil surface, this technique is not reliable due to air contribution in the sampling volume [33]. The neutron probe sounds free water and bound water trapped in clay minerals, whereas other techniques such as GPR only account for free water. To remove the contribution of bound water, models that estimate the quantity of bound water for a specific texture and bulk density are used. The neutron probe is

labour intensive, costly, and requires precaution upon handling radioactive material [31] [34] [35].

2.3.3 Remote sensing

Remote sensing comes as a method of SWC monitoring at the catchment scale. At this scale, surveillance is of interest to determine the separation of precipitation into infiltration, evapotranspiration, and run-off. This quantification serves for modelling soil water erosion and river discharge. Remote sensing can be satellite-borne or air-borne. When measuring from large distances, the penetration depth tends to be very narrow (only surveying the top 5 centimetres for example) and there is usually a large influence of vegetation on the data.

2.3.4 Electromagnetic methods

Electromagnetic methods to estimate soil water content are dependent on the high correlation between relative dielectric permittivity (ϵ_r)and water content (θ_v). These methods include time domain reflectometry (TDR), electromagnetic induction (EMI), electrical resistivity tomography (ERT), synthetic aperture radar (SAR) and ground penetrating radar (GPR) which will all be discussed in the next sections.

2.3.4.1 Empirical relationships between θ_v and ϵ_r

Topp's empirical equation (eq. 2.5) between apparent permittivity and soil water content is the most widely used. In this situation, ϵ refers to an apparent permittivity because it was determined from wave velocity in the soil [36] [37]. This polynomial relationship has been determined to be appropriate for large ranges of soil moisture contents with a prediction error of 0.013 m^3/m^3 [33].

$$\theta_v = -5.3 \times 10^{-2} + 2.92 \times 10^{-2}\epsilon - 5.5 \times 10^{-4}\epsilon^2 + 4.3 \times 10^{-6}\epsilon^3 \tag{2.5}$$

The dielectric mixing model (eq. 2.6) provides a more physical link between θ and ϵ. This model is build on the permittivity of every soil component and the fraction of volume it occupies to derive a bulk permittivity of a soil-water-air mix (ϵ_b) [37] [33].

$$\epsilon_b = [\theta \times \epsilon_w^\alpha + (1-n) \times \epsilon_s^\alpha + (n-\theta) \times \epsilon_a^\alpha]^{1/\alpha} \tag{2.6}$$

With,
n = the soil porosity
ϵ_w = permittivity of water
ϵ_s = permittivity of soil particle
ϵ_a = permittivity of air
α = a factor "accounting for" the orientation of the electrical field with respect to the geometry of the medium ($\alpha = 0.5$ for an isotropic medium)

The third petrophysical relationship between θ_v and ϵ_r is the effective medium approximation. This method takes textural and structural contribution into account [33].

Because most of the calibrations between ϵ and θ were derived using TDR, in its range of $\pm$ 500-1000 MHz, caution should be taken when operating outside this range. In that case, site specific calibration might be required, implying many auxiliary measurements [37]. Pre-established petrophysical relationships based on experimental data, volumetric mixing formulae using component electrical properties and effective medium approximations based on geometrical models have however proved themselves acceptable in a wide range of conditions and set-ups [33].

2.3.4.2 Time Domain Reflectometry

TDR probes measure the effective dielectric permittivity over the length of the probe. Wave propagation is guided and is one dimensional. This method results in shallow VSWC estimation at the point scale, it is reliable and can easily be automated, it is also a worthwhile technique for it is capable of simultaneously measuring bulk soil conductivity and dielectric permittivity [37]. However, this technique is labour intensive and it is prone to errors due to air gaps between the probe and the soil if carelessly inserted in the soil [31]. There is a question of representativeness because of the small measurement volume.

2.3.4.3 Electromagnetic Induction

EMI characterisation uses low frequencies in the range of kilohertz. Consequently, the measurement is highly sensitive to soil electrical conductivity. The penetration depth is quite large and the total sampling volume as well.

2.3.4.4 Electrical Resistivity Tomography

ERT is a method of injection of a current into the soil using two probes, and two other probes receive the reflection in order to quantify the soil's resistivity, the inverse of the electrical conductivity. This method requires a contact between the soil and the probes. The result is a mean electrical conductivity over a large sampling volume.

2.3.4.5 Synthetic Aperture Radar

SAR is an electromagnetic remote sensing method which uses overlapping data. A post processing is necessary to create a narrow beam and achieve $\sim$15m resolution from a satellite measurement.

2.3.4.6 Ground Penetrating Radar

The Ground Penetrating Radar is very promising for soil moisture monitoring because it fills the scale gap between point scale measurements (TDR, gravimetry,..) and catchment scale (remote sensing). Indeed, it uses an intermediate scale, the scale of agricultural plots [37]. GPR

is also promising for it's non destructive but high resolution exploration of the soil. GPR will be further explored in the next chapter.

A short table below synthesises all SWC monitoring methods that were discussed before with their scale of investigation, as well as the pros and cons for their use.

Method	**Scale**	+	-
Gravimetric and volumetric SWC	Point	Direct, simple, highly precise	Destructive, time consuming
Neutron probe	Variable	Accurate, can be used in real time	Complicated characterisation scale, labour intensive, costly, ineffective for top of soil profile, requires calibration, cautious handling
Remote sensing (SAR)	Catchment	Rapid data acquisition	Small penetration depth, large influence of vegetation
TDR	Point	Reliable, easily automated, simultaneous ϵ_r and σ measurement	Sensitive to quality of insertion, representativeness
EMI	Catchment	Non-invasive, fast	Large sampling volume and depth
ERT	Catchment	Requires good contact between soil and antenna	Large sampling volume and depth
GPR	Field	High resolution, non destructive	Difficulties with slopes and high conductivity soils

Table 2.1: Soil water content monitoring methods.

Chapter 3

Ground Penetrating Radar

3.1 Electromagnetic principles

The Ground Penetrating Radar is a geophysical method of investigation of the soil below it's surface, considering the soil to be a dielectric material. Imaging the subsurface is based on the propagation and reflection of electromagnetic waves in the soil, governed by Maxwell's equations. GPR uses high frequency waves in the relatively narrow range of more or less 50 to 1500 MHz to probe the subsurface [38].

Three electromagnetic properties of the soil are given below. They describe the material's response to the electromagnetic fields [39].

1. Dielectric permittivity ϵ_r : characterizes the polarizability of a dielectric relative to vacuum permittivity (eq. 3.1) and modulates wave velocity (eq. 3.2).

2. Electric conductivity σ : characterizes free charge movement and impacts wave attenuation.

3. Magnetic permeability μ : characterizes the degree of induced magnetism due to a magnetic field. It is usually not of interest in GPR applications and approximated as free space permeability.

$$\epsilon_r = \frac{\epsilon}{\epsilon_0} \tag{3.1}$$

With,
ϵ = the absolute permittivity (F/m)
ϵ_0 = the permittivity of vacuum ($\epsilon_0 = 8.89 \times 10^{-12}$ F/m)

$$\epsilon_r = (\frac{c}{v})^2 \tag{3.2}$$

With,
c = speed of wave in a vacuum / speed of light ($c = 3.10^8$ m/s)

v = speed of wave in the dielectric medium (m/s)

The dielectric permittivity of a soil is a complex, frequency-dependent number (see eq. 3.3). The real part $\epsilon'(f)$ is associated with the capacity of energy storage under an alternating electrical field and the imaginary part, $\epsilon''(f)$ is the component of energy dissipation [39] [37]. The dielectric losses (dispersion of permittivity) are centered around a specific frequency, the frequency of relaxation, according to the model of Debye [37]. However in the GPR frequency range, $\epsilon''(f)$ is often negligible compared to $\epsilon'(f)$, because center frequency of relaxation of water is around 17 GHz at 25°C, way above GPR frequencies.

$$\epsilon(f) = \epsilon'(f) - j\epsilon''(f) \tag{3.3}$$

Generally, the GPR response is widely influenced by the content of water in the soil, given the fact that water is by far the most polarizable material of the soil, with $\epsilon_r = 80$. As a result, GPR can be used to quantify soil moisture. Alike other electromagnetic methods (Time Domain Reflectometry, Electromagnetic induction, Single Aperture Radar,...) it uses the high correlation between relative permittivity of the soil and it's water content which is translated into empirical equations such as Topp's or other mathematical relationship between θ_v and ϵ_r [36] [40] [39] (see chapter 2, section 2.3.4.1). This paper focuses on this quantitative use of the GPR while the qualitative use (subsurface imaging) is not investigated.

The resolution of the GPR measurement is determined by the period of the emitted wave, which itself depends on the bandwidth of the GPR [37]. Furthermore, a higher frequency GPR will yield a higher resolution [41].

Regarding probing depth, the penetration of the electromagnetic waves is determined by the soil electrical conductivity and the center frequency of GPR system. Probing depth increases when conductivity decreases due to the attenuation of the wave caused by electrical conductivity. In low-electrical-loss materials ($\sigma \to 0$), the signal penetrates to a great depth. In practice, soils do not have $\sigma = 0$, and clay or saline soils especially will have a limited depth of penetration [40]. Depth penetration is also frequency dependant : in a sandy soil at 100 MHz it will reach several 10 meters but only several meters at 450-900 MHz [37].

3.2 Survey methods : systems and designs

Obtaining information about the soil using GPR and radio waves can be done according to multiple different methods. The different methods can survey surface or subsurface properties, they can be on-ground or off-ground, use the reflection or transmission of electromagnetic waves. The soundings can be performed in the time domain or in the frequency domain, and a variety of different antenna types can be used.

Time domain GPR, also known as impulse radar is the most common. A short impulse is emitted, and it can clearly be caught by the receiving antenna when the pulse duration or width is short and the amplitude is large.

Frequency domain is set up as a continuous wave (CW) made of a sum of sinusoids each having their own frequency. When adding a high number of signals, the frequency domain radar approaches a short pulse.

3.2.1 Ground wave

The velocity of the ground wave, retrieved as a result of propagation time measurements between two antennas gives an estimation of soil water content through dielectric permittivity. The ground wave travels in the shallow subsurface from an on-ground transmitter to an on-ground receiver [38] [42].

$$v = \frac{L}{t_{gw}} \tag{3.4}$$

With,
v = ground wave velocity (m/s)
L = distance between transmitting and receiving antenna (m)
t_{gw} = direct ground wave travel time (s)

This method gives a reading of the shallow water content, which can be of interest for vadose zone process comprehension in hydrological models. Instead of classical methods such as gravimetry or TDR, ground wave GPR results in a much denser sampling in order to adequately cover the spatial variability of moisture content, and it is less time consuming. This can be especially interesting in a vineyard for example where spatial variability is important due to topography and where moisture content has an acute impact on grape quality [38].

Surface GPR ground wave method can be realised using three survey types : common midpoint (CMP), wide-angle reflection and refraction (WARR), and fixed offset (FO) [42]. The vertical resolution of a GPR ground wave method will not be very different from a TDR or oven drying survey, but the lateral resolution will be much larger [38].

Common midpoint : Using multiple measurements with different antenna separations on one transect, the transmitter and receiver are displaced progressively away from each other, keeping the midpoint at a set position. The travel time increases with each measurement.

Wide-angle reflection and refraction : This technique is also a variable offset method, but with a fixed position for the transmitting antenna. Variable offset is time consuming and it has a large sampling volume, implying a lower spatial resolution.

Fixed offset : In this case, the antenna separation is constant. The transmitter and receiver are moved in parallel along a transverse.

The travel time of the ground wave is established from the subtraction of "time zero", the arrival time of the air wave travelling at the speed of electromagnetic waves in a vacuum c. Using the distance between transmitter and receiver and the travel time, the speed of the ground wave is found and can be used in equation 3.2 to estimate dielectric permittivity. This approximation is valid for high frequencies and low electrical conductivities [38]. On a radargram (fig. 3.1), the slope between the ground wave travel times and the antenna separations is used to retrieve ground wave speed in a variable offset mode, and arrival times for the air wave and the ground wave are used in a fixed offset mode.

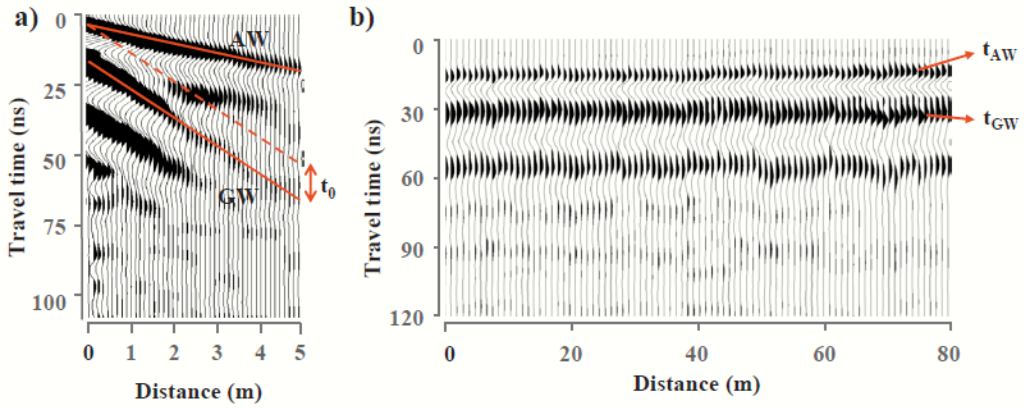

Figure 3.1: Radargram for a) CMP and b) FO GPR surveying (aw = air wave ; gw = groundwave) [43].

3.2.2 Surface reflection coefficient

In this configuration, the determination of the dielectric permittivity is based on the assessment of the reflection coefficient at the soil surface interface and it retrieves soil surface water content [44]. There is a correlation between the difference of permittivities between air and soil and the reflection. Six assumptions are made to use the surface reflection coefficient method :

1. The antennas are off the ground, in free space above the soil surface. The interface is plane and the soil is homogeneous.
2. The reflection coefficient may be approximated by the plane wave reflection coefficient.
3. Antenna distortion effects are negligible.
4. The soil electrical conductivity σ is negligible.
5. The magnetic permeability μ is equal to the free space permeability μ_0.
6. The dielectric permittivity is independent from frequency.

Considering these six hypotheses, equation 3.5 can be used to retrieve permittivity from surface reflection coefficient. This surface reflection coefficient is determined by the measured amplitude of the surface reflection A relative to the amplitude measured for a perfect electric conductor (metal plate) situated at the same distance as the antenna to the soil, A_{PEC} (see eq. 3.6 and 3.7) [44] [37].

$$\epsilon_r = (\frac{1-R}{1+R})^2 \tag{3.5}$$

With,
R = the amplitude of the reflection coefficient

$$\frac{R}{R_{PEC}} = \frac{E_s/E_i}{E_{s,PEC}/E_i} \tag{3.6}$$

With,
R_{PEC} = -1
E_i is assumed constant
A (measured) is directly proportional to the backscattered electric field $E_s \rightarrow$ there are no antenna distortion effects

$$R = -\frac{E_s}{E_{s,PEC}} = -\frac{A}{A_{PEC}} \tag{3.7}$$

3.2.3 Propagation time to a known interface

Reflected wave velocity is a method where partial reflections at dielectric contrasts are recorded. Given that GPR emits in all directions, reflections appear before and after being above the reflector when displacing the GPR along a transect resulting in a hyperbola shaped position-travel time GPR response. The shortest travel distance (and time) is logically when sounding directly above the reflector. This method uses known reflectors, such as a thin low permeability clay layer that was identified and mapped through boreholes, to retrieve the speed of the wave using equation 3.8 or the convexity of the reflection hyperbola [37].

$$v_{soil} = \frac{\sqrt{(x-0.5a)^2+d^2} + \sqrt{(x+0.5a)^2+d^2}}{t_{rw,x}} \tag{3.8}$$

When the depth of the reflecting interface is unknown, a variable offset mode is used such as CMP or WARR using equation 3.9 (see fig. 3.1). With this method, we can calculate an average dielectric constant for the portion of soil above the reflector using the two way travel time to the interface [31] [37]. This leads to a large sampled area.

$$v_{soil} = \frac{2\sqrt{(0.5a)^2+d^2}}{t_{rw,a}} \tag{3.9}$$

With,
x = the position relative to the position of the scattering object (minimum of the hyperbola)

d = the depth of the scattering object
a = antenna separation
$t_{rw,x}$ = the arrival time of the reflected wave at position x with time zero correction

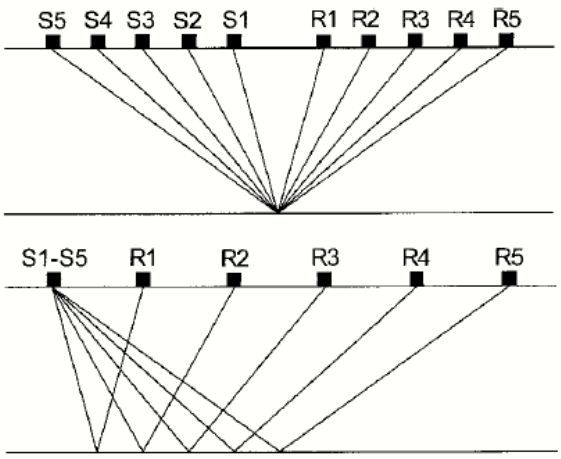

Figure 3.2: Variable offsets. CMP (top) and WARR methods (bottom). S = transmitter and R = receiver [37].

3.2.4 Borehole GPR

Surveys using the transmission of electromagnetic waves instead of their reflection are usually carried out in boreholes. In this survey mode, the two antennas are placed in access tubes. The methodology is similar to previous GPR techniques, relying on propagation time between boreholes to determine speed and hence permittivity. This technique is less common.

3.3 Antennas

Antennas transform an electrical signal generated and received by the VNA to and from vector electromagnetic fields propagating usually in the air. The transmitter antenna creates and the receiver antenna detects the fields [45]. In bistatic mode, one antenna serves as transmitter and a second one as receiver whereas only one antenna fills both roles in monostatic mode.

Bandwidth The bandwidth of the radiated energy is equivalent to the range of frequencies.

Directivity Directivity is the ratio between the maximal and the average power density. In a certain direction, the power received or transmitted per unit solid angle is compared to the average power over a unit solid angle. Usually directivity is defined for its maximum in the main beam axis [46].

3.3.1 TEM horn antenna

The transverse electromagnetic horn antenna (TEM horn) is an extension to the waveguide made of metal sheets (see fig. 3.4) [47]. Previously used in drone-borne GPR applications [48],

the TEM horn was used for its high directivity, making it adapted to off-ground measurements [49]. Consequently, measurements had a high resolution and more information about subsurface properties was derived. Directivity is especially high at high frequencies, and if the antenna is filled with a dielectric, a high bandwidth is achievable without needing important antenna dimensions. Used in monostatic mode, only one TEM horn is used as transmitter and receiver[50].

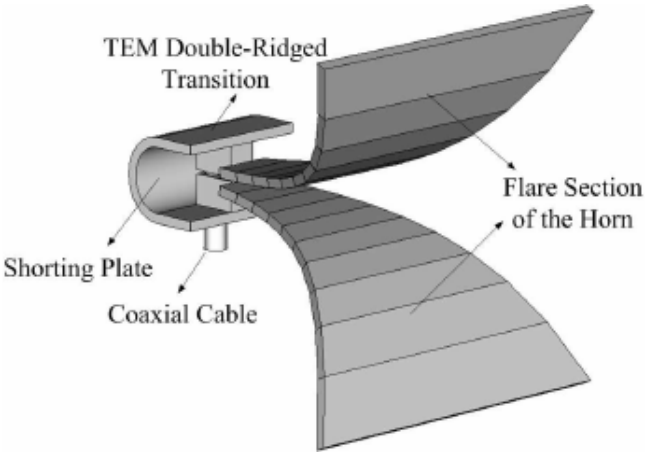

Figure 3.3: Configuration of a TEM horn antenna [51].

3.3.2 Dipole antenna

The dipole antenna is common for its simple design. It is made of two wires, measuring in total half the wavelength of the required frequency. Hence it also being called half-wave dipole antenna. The conductor is interrupted in the middle [52]. Dipole antennas have a much lower directivity than the horn. The radiation pattern is donut-shaped and the polarization is linear [53].

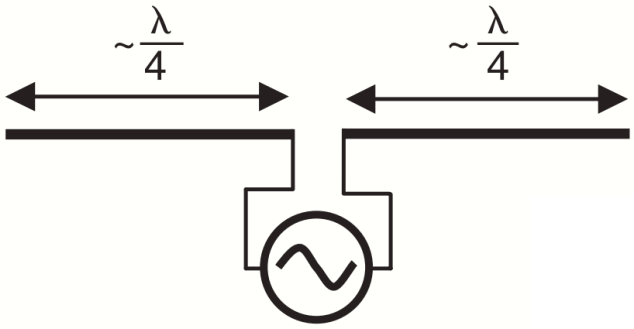

Figure 3.4: Configuration of a dipole antenna [53].

3.4 Full wave inversion

Full-wave inversion is used to determine quantitative values of electromagnetic properties such as the dielectric permittivity [48]. Using the radar equation of Lambot, it is possible to accurately model the GPR signal and filter antenna effects in the frequency domain [54] [55].

Equation 3.10 describes the ratio between the transmitted and received wave in the far field (transmitter and receiver assumed to be in a same point) [56].

$$S_{11}(\omega) = \frac{b(\omega)}{a(\omega)} = R_i(\omega) + \frac{T(\omega).G_{xx}(\omega)}{1 - R_S(\omega).G_{xx}(\omega)} \tag{3.10}$$

With,
$S_{11}(\omega)$ = Measured raw radar data
$a(\omega)$ = Transmitted wave
$b(\omega)$ = Received wave
$R_i(\omega)$ = Antenna global reflection coefficient for the incident field (free space antenna response)
$R_S(\omega)$ = Antenna global reflection coefficient for the reflected field
$T(\omega)$ = Product between antenna global transmission coefficients for the incident and reflected fields
$G_{xx}(\omega)$ = Green's function describing the reflected electric field in 3D multilayered media

The inversion consists of minimising the objective function (eq. 3.11) which is defined as the difference between the observed radar signal and the modelled radar signal for a specific set of parameters. This optimisation can be realised using algorithms such as a global multilevel coordinate search or a local Nelder-Mead Simplex algorithm but in this case, a look up table (LUT) is used [49]. The look up table computes the objective function fully for all antenna heights and soil dielectric permittivities. This approach ensures that the global minima is reliably found and enables the inversion to be made in real time [48].

$$\phi(b) = (g_{xx}^{\uparrow *}(t) - g_{xx}^{\uparrow}(b,t))^T (g_{xx}^{\uparrow *}(t) - g_{xx}^{\uparrow}(b,t)) \tag{3.11}$$

With,
$g_{xx}^{\uparrow *}(t)$ = Measured Green's function in the time domain (found through the inverse Fourier transform)
$g_{xx}^{\uparrow}(b,t)$ = Modelled Green's function in the time domain

Chapter 4

Positioning

4.1 GNSS

GNSS, or global navigation satellite system is a system of geo-spatial positioning with global coverage, some of the most well known GNSS are GPS (USA), GLONASS (Russia), BeiDou (China) and Galileo (Europe). Determining geographical positioning using a GNSS receiver uses information from satellites that are continuously transmitting their exact position at each moment in time. These signals are used by the GNSS receiver to locate itself in space. The device receives a signal, and using its own internal clock, it measures the time of reception of the signal. With the hypothesis that there are no GNSS errors, the device determines the time it took for the signal to reach the receiver. Given that we know the speed of the signal, since it is the speed of light, we can determine the distance travelled by the signal. Using triangulation, three different satellite signals should theoretically suffice to find the exact position of the receiver, assuming that one of the two points of intersection can be excluded when it is beneath the soil surface or in outer space. In practice, a minimum of four signals are required in order to minimise the error due to the lesser accuracy of the receiver's clock. Indeed, receivers use quartz crystal clocks which have a much lower precision than atomic clocks used by satellites. Generally, the more satellites used, the more accurate the estimate of the GNSS receiver's position [57].

Galileo, the European global satellite based navigation system consists of a constellation of 24 operational satellites and 6 spares, all on three orbital planes at 23 000 km above the earth's surface. Unlike GPS and GLONASS, Galileo is under civilian control, while the two others are military, providing reliability to Europeans. Generally, on earth, six to eight satellites will be visible, resulting in a high precision of location and time. The relative position of the satellites used by the GNSS is quantified by the geometric dilution of precision (GDOP). When GDOP is bad, the satellites used by the GNSS receiver make a small angle with the receiver and this results in less accuracy [58].

4.2 GNSS augmentation

Although GNSS is very useful today, it is quite inaccurate. There is a typical offset of 2-3m but the error can reach 10m. This precision is usually sufficient for navigation, but for high precision applications an augmentation of GNSS is necessary [59]. GNSS technology can be enhanced by an aircraft-based augmentation system (ABAS), a satellite-based augmentation system (SBAS), or a ground-based augmentation system (GBAS). All three are systems designed to improve the georeferencing accuracy and reliability.

ABAS is mainly used for aviation applications using on-board information. SBAS includes the European Geostationary Navigation Overlay Service (EGNOS) for Galileo in Europe and Wide Area Augmentation System (WAAS) for GPS in the United states. Other geographical areas have their own SBAS, but all are compatible and interoperable [58]. SBAS enhances accuracy and reliability by two means, first by providing a correction and second by providing information about the accuracy, integrity, continuity and availability of its signals. SBAS functions using GNSS measurements taken by reference stations deployed across the planet. All measured GNSS errors are sent to a central computing centre, where differential corrections and integrity messages are calculated. Then, geostationary satellites broadcast these calculations which will be used by GNSS users as an augmentation of the initial GNSS information [58].

Differential GNSS (dGNSS) is a ground-based augmentation system (GBAS) which provides differential correction and integrity monitoring to GNSS [60]. The method used by dGNSS is to assume that the atmospheric correction should be the same for both receivers (base and rover) when they are geographically close (± 100 km) and to use the known location of one receiver (base) to determine the correction to be made to the second receiver (rover) (see fig. 4.1) [61] [62].

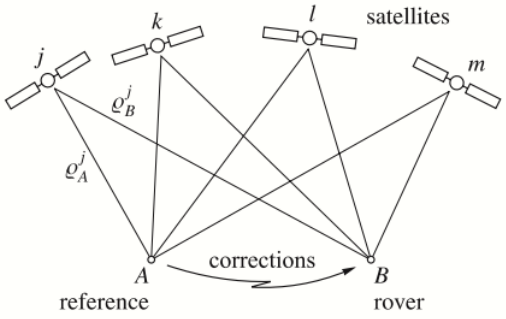

Figure 4.1: Differential positioning using four satellites and two GNSS receivers [62].

The differential correction can be applied in real time with what is called Real Time Kinematic (RTK) or as a post processing technology like Post Processing Kinematic (PPK). The correction can be sent by radio waves or over the internet with the NTRIP protocol to provide real time communication between base and rover.

4.2.1 Post processing kinematics

Post processing kinematic (PPK) is a method of differential correction where all raw measurement data is recorded on the receivers and is processed afterwards to get centimetre precision. In this case, no real time connection is required between the base and the rover. Data from both is saved in logs and it is processed after data acquisition. This method is often used in UAV mapping and as a back-up for RTK. Setup is simpler than RTK and it is useful in photogrammetry for not requiring ground control points (GCP). The advantage is also that there is no risk of loss of data because of a connection fault [57] [63].

4.2.2 Real time kinematics

This technology enables a GNSS receiver (the rover) to receive data from a second GNSS receiver (the RTK base station) in real time, either by radio waves or with the internet with the NTRIP protocol. The advantage of real time is balanced with the risk of failure if connection is lost between base and rover. This mandatory connection between base and rover also puts a limit on the size and terrain of the investigated area.

4.2.3 Correction transmission over NTRIP

With NTRIP (Networked Transport of RTCM via Internet Protocol), the rover can access data for its correction from a local provider's RTK base station with centimetre accuracy. In order to have an internet connection, the GNSS receiver will be equipped with a SIM card and mobile data. The NTRIP protocol was released in 2004 by a German organisation. The principle is that local organisations share their base stations over the internet, and anyone can borrow them. It that case, you can operate RTK with only one GNSS receiver.

4.2.4 Data transmission over LoRa radio

LoRa, or Long Range radio is a low-power wide-area network (LPWAN) protocol developed by Semtech. Widely used for Internet of Things (IoT) applications in smart cities, smart buildings, smart agriculture, and more, connecting diverse devices to their networks [61].

In the transmission of a correction from base to rover, LoRa radio has several advantages over internet which are power consumption, a greater range, and a secure transmission. This technology by Semtech has revolutionized Internet of Things by providing data communication over a long range but consuming limited power [64] [65]. LoRa enables a connection up to 19km distance when visibility is good and a few km in urban areas with only 20 dBm power output [57]."

The LoRa radio can be configured as emitter or receiver, but it can only work in one way. The base GNSS module will be configured to send corrections and the rover module to receive them.

4.2.5 Setting up the base station

Base should be set up first so it can transmit the corrections to the rover. With EMLID Reach RS+, there are four different methods of setting up an RTK base station using the Reachview application [57].

1. **Manual** : The base is set up on a trig point, which is a marked point with certified coordinates. The base station's coordinates are then manually input in the Reachview app using WGS84 latitude and longitude and WGS84 ellipsoid height, taking care to add the altitude difference between the marker and the antenna. With this approach, absolute accuracy depends on how accurately the trig point's coordinates were determined, and relative accuracy is centimetric.

2. **Averaged single** : In this method, the base station's position is determined with an accumulation of coordinate measurements over a chosen period of time (5 minutes for example) and might have an offset of a couple of meters. The relative position of the rover will still be centimetre precise but the absolute precision is limited by the accuracy of the base station's positioning. This method results in a constant shift of rover coordinates and meter level absolute accuracy.

3. **Averaged fix** : If enough satellites are visible by the receiver, the average method can provide a fixed solution for the ambiguity resolution. The ambiguity resolution is an algorithm to calculate the exact number of radio wavelengths between the base station and the satellites. In a fixed solution, there is a whole number of wavelengths. Typically, in order to work in this mode, the base receives NTRIP corrections over the internet and broadcasts it for the rover [66].

4. **Averaged float** : If insufficient satellites are in sight, RTK only provides a float position, precision is less than with fixed solution but still better than without differential correction. The float solution allows the ambiguity to be a decimal or floating point number.

In any case, the rover's position is centimetre precise relative to the base when the distance between both is reasonable (under 10 km).

4.3 EMLID dGNSS

In a very recent study, two low cost RTK GNSS's were compared. Emlid GNSS was found to have superior localization performance than NavSpar, with 94% versus 71.5% of data in fixed solution. However both were found to be promising for precision applications such as soil moisture mapping using a drone-borne GPR [67].

Chapter 5

Soil moisture mapping using a drone borne GPR

5.1 Materials and methods

5.1.1 Study site

The studied field is an agricultural plot located in Gembloux, Walloon Region in Belgium. The Geographical coordinates of the approximate center of the studied field are 50°33'47" N and 4°43'55" E. The sounded area is about 16135 squared metres (1.6 ha). The altitude is of 165 metres and only a very slight slope is observable. The numerical map of Walloon soils (CNSW) indicates that the soil is loamy throughout the whole sounded area, with varying drainage and some gleyed soil (see fig. 5.1). During the measurement campaign, the soil was covered with wheat.

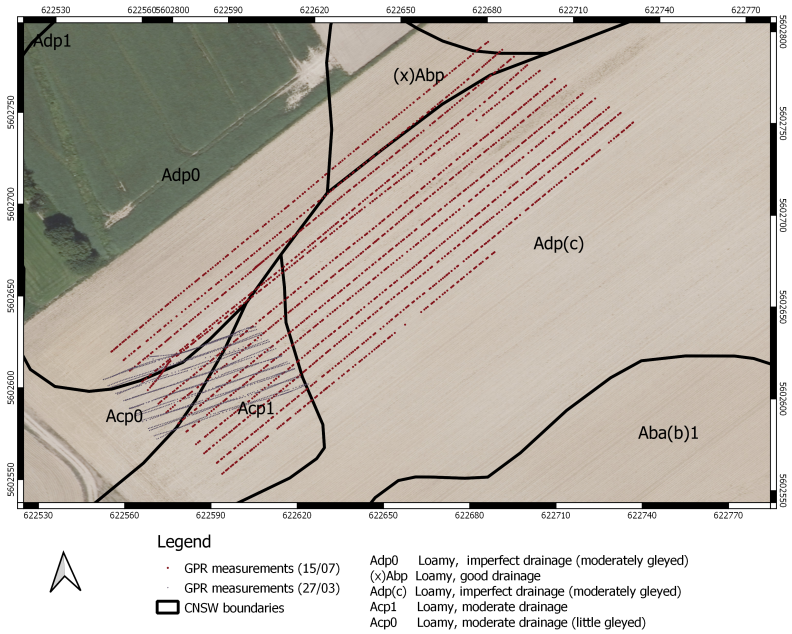

Figure 5.1: Study site in Gembloux for the fwo measurements campaigns. Coordinates are in Lambert Belge 72 (m). WGS84 DATUM

5.1.2 Experimental setup

Mounted on an RCTakeoff X8 drone, the ground penetrating radar is made of a lightweight vector network analyser (VNA) and a monostatic dipole antenna of 50 cm. It is connected to a Reach M+ GNSS receiver, and a compute stick (see fig. 5.2).

Figure 5.2: Drone-borne ground penetrating radar setup.

For centimetre precision, the REACH M+ UAV mapping kit was used from EMLID for the drone borne GPR application. This kit comprises an EMLID REACH RS+ GNSS receiver, an M+ RTK GNSS module, a LoRa radio and a GNSS antenna for about $1000 (see figure 5.3).

The kit comes with a mobile application called ReachView designed for collection of points and control of the device. To reach centimetre precision, reach RS+ uses RTK technology. The two receivers communicate with LoRa radio, Reach RS+ has an internal LoRa radio while Reach M+ uses an external LoRa radio which can be connected via USB or S1/S2 port. Reach RS+'s internal radio will broadcast RTK corrections while Reach M+'s LoRa receives them.

Figure 5.3: EMLID Reach M+ UAV mapping kit.

In field, Reach RS+ is mounted on a tripod, preferably in an open area. the tripod needs to be levelled accurately. Without an available trig point, the average method is used to set up the base station. Reachview app will display whether base was set up in average single, average float or average fixed. In single mode, base corrections are not applied, float mode considers base corrections, and fixed mode means all ambiguities are resolved and RTK solution

is centimetre level accurate. Normally, after a while, the rover will get a fixed solution and data acquisition may start [57]. Reach works well in tough outdoor conditions, it is waterproof, it has 22 hours of battery, it is impact resistant, the set up is simple and it is easy to operate [57].

5.1.3 Data Acquisition

The drone is able to fly in automatic mode using the Cube Autopilot flight controller. In this mode, a predefined trajectory is encoded and a stable flight with limited changes in incidence angle caused by acceleration, a more regular sampling grid and less laborious data acquisition is possible. The drone is also coupled with a QGround Control system, which allows it to fly at a defined height above the soil surface. This system uses a LIDAR (Garmin optical sensor) which continuously measures the drone's flying height. To obtain quality radar data, the drone should fly at about 3 meters above the ground. At this altitude, the GPR will still be in the far field, and thus respect the hypotheses of the radar model and it will be close enough to obtain a good signal to noise ratio. This desired altitude also depends on the slopes of the studied field. For security reasons, if abrupt slopes are present on the study site, a higher flying mode might be necessary depending on the speed at which the QGround control adapts the flying altitude. The topic of the ideal flying height still deserves a more in depth study.

For each measurement, the VNA transmits a stepped frequency continuous wave (SFCW) to the dipole antenna, with a direct connection, preventing dielectric losses from coaxial cables. Subsequently, the VNA is capable of measuring a reflection coefficient in an ultrawide band in order to reach different characterisation depths. For each radar measurement, a dGPS measurement is associated. These two measurements are linked by the exact time at which they are taken in the matlab codes [1].

Before operating the radar, a choice of bandwidth is realised by arbitrarily choosing to keep frequencies for which R_i (the free-space antenna response) is lower that 0,5. In this range of frequencies, minimum 50% of the energy is transmitted towards the ground instead of being directly reflected inside the VNA.

In order to retrieve the free-space response, a high altitude is reached before engaging in the automatic grid of points. The measurements taken at a high altitude are useful because in this zone, Green's function is equal to zero and the VNA measures the free-space response ($S_{11} = R_i(\omega)$).

Out of all sensor measurements, the ones taken during a change of direction and during the initial high altitude of the drone should not be considered for the map. Changes of direction imply changes of incidence angles for the radar and high altitude implies a very low signal to noise ratio. Therefore, an arbitrary area is delineated by the user, in order to select data of

[1] Matlab codes not included in appendix because they are confidential

interest for the soil moisture map.

5.1.3.1 Primary dataset : 15/07

The main dataset used in this study was taken on July 15th 2020 (see red points in fig. 5.1). 3800 measurements were taken on an area of about 1.6 ha (0.24 $measurements/m^2$) and the flight took 14 minutes. A frequency range of 234-335 MHZ was used to respect $R_i < 0.5$ and a frequency step of 1 MHz was used, which yields a total of 100 frequencies.

Unfortunately, there was an accident due to poor security settings and the drone crashed while returning to it's take off position. The threshold set for an automatic return was set too low. Radar measurements however were still running for another 12 minutes while the drone was recuperated. On figure 5.4, the altitude of the VNA is plotted for all measurements. the first peak is voluntary, the second peak around point index 4000 corresponds to the drone's return to base technique which was interrupted by the crash and all measurements after index 4000 shouldn't be considered since they were taken while the drone was not flying. Out of a total of 7154, only 3800 measurements are considered to be part of the mission.

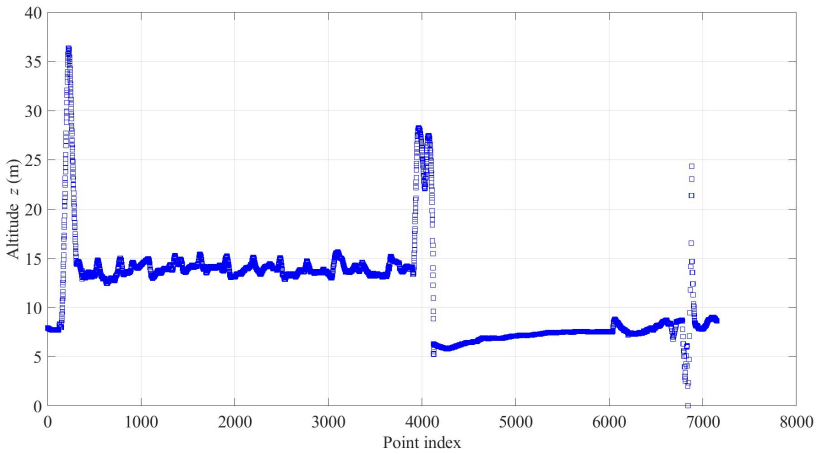

Figure 5.4: Altitude of all measurements : 15/07.

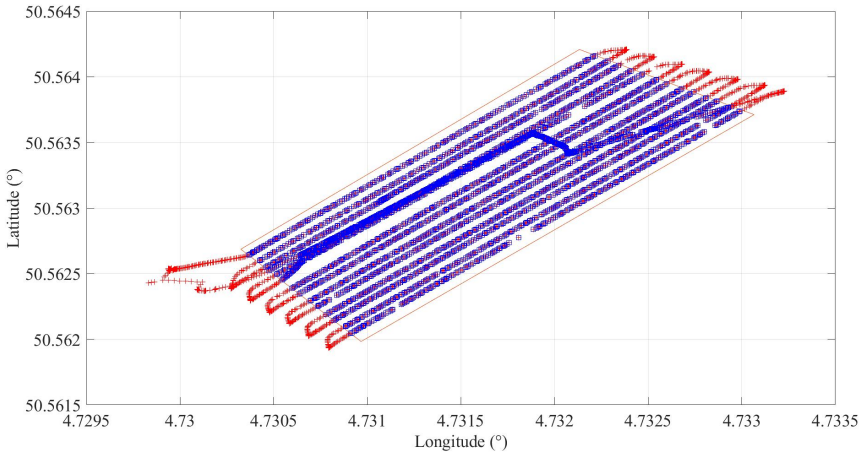

Figure 5.5: Map of all measurements : 15/07. The blue polygon shows the selection of points excluding changes of direction. Latitude and longitude are in decimal degrees (WGS84).

The drone reached 36 metres of altitude (first peak see fig. 5.4) before engaging in its automatic grid. Arbitrarily, all measurements above 30 metres were selected to be used as free-space response. As visible on figure 5.5, From the initial 3800 measurements, only 2760 were kept after selecting of the blue polygon.

5.1.3.2 Secondary dataset 27/03

On March 27th 2020, measurements were taken on the same agricultural plot using the same drone-GPR setup (see brown dots in fig. 5.1). A much smaller area (2354 m^2) was sounded and the drone flew significantly lower. In 21 minutes, 6165 radar measurements were taken, which results in a much denser grid of data (2.62 $measurements/m^2$). For this flight, a range of frequencies of 440-640 MHz was used to respect the $R_i < 0.5$ criterion. The high altitude measurements were selected from 16 meters to retrieve free-space response (see fig. 5.6) . After delineating an area of interest (excluding changes of direction and high altitude measurements), only 1893 measurements were left (see fig. 5.7).

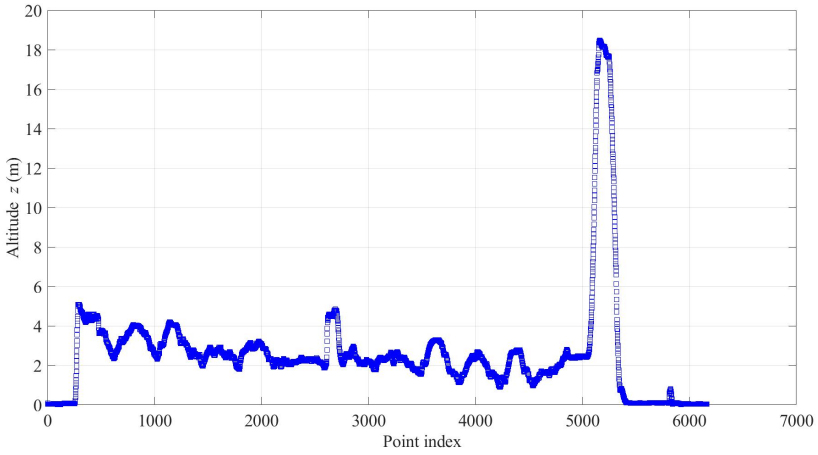

Figure 5.6: Altitude of all measurements : 27/03.

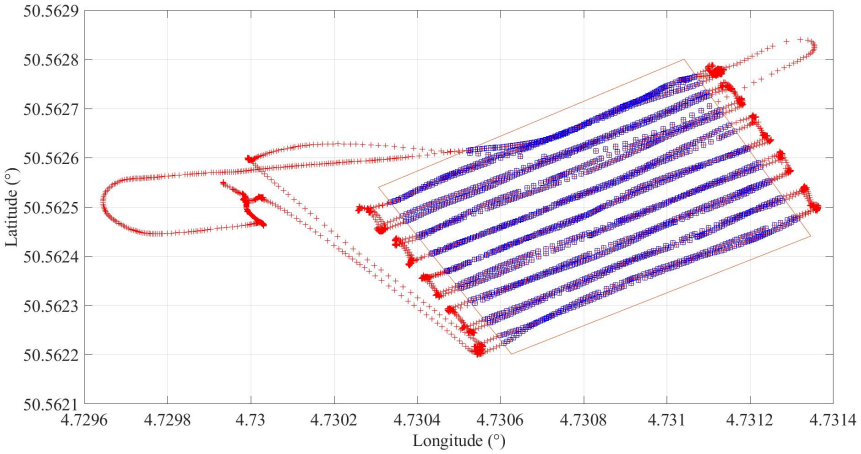

Figure 5.7: Map of all measurements : 27/03. The blue polygon shows the selection of points excluding changes of direction. Latitude and longitude are in decimal degrees (WGS84).

5.1.4 Antenna calibration

In order to characterise the antenna's properties, measurements are made at different heights above a body of water. By measuring S_{11} and solving a system of equations (eq. 3.10) $R_i(\omega)$, $R_s(\omega)$ and $T(\omega)$ (the antenna transfer functions) can be determined. Three configurations are necessary to solve the system, but here an overdetermined system of equations is used with 5 measurements at 5 different heights, yielding a better solution [68].

Upon solving this system of equations, far-field antenna effects can be filtered out from the radar data. It is important to calibrate the antenna while it is mounted on the drone, because of possible interactions from the blades and carbon structure [48].

5.1.5 Inversion

The inversion is performed in the time domain for far-field radar data. First, a look-up table (LUT) is established of simulated radar data (S_{11}) in the frequency domain, for a range of heights and dielectric permittivities using the far-field antenna model of Lambot. These simulations are made with the a matlab code which is an electromagnetic model that calculates the Green's function. The model considers a planar layered medium with one layer of air and only one layer of soil. For relatively high frequencies (234 - 335 or 440 - 640 MHZ), the electric conductivity is considered to have no effect on the reflection coefficient at the soil surface. Consequently, the model calculates the signal for only two parameters : a given altitude and a dielectric permittivity. In this case, antenna heights were taken between 3 and 9 metres (1 and 6 metres for the 27/03 dataset) with a step of 0.01 m while the second parameter, ϵ_r went from 3 ($\sim$ dry sand) to 25 ($\sim$ completely saturated) with a step of 0.5 (corresponding to 1% of SWC). The choice of altitude range is realised using the graph of measured signals in the time domain (see section 5.2.2 figures 5.10 and 5.11). Thus a total of 27045 simulated radar measurements (22545 for the 27/03 dataset) are computed and saved. In matlab code, this operation computes about 10 radar signals per second. This step corresponds to the forward model.

After filtering out antenna effects, the inversion is performed on the Green's function. For each of the measurements, an objective function, defined as the difference between the modelled and the measured Green's function is calculated for each of the simulations in a LUT. A search algorithm sweeps through the LUT and selects the height and dielectric permittivity for which the objective function is minimal for each measurement. This least squares process inverts about 300 measurements per minute. This optimisation is simpler and more robust with a LUT because every possible combination of parameters is tested and the modelled data is computed only once for all measurements. The output is a grid of dielectric permittivities for each radar measurement on the test site.

5.1.6 Exclusion based on objective function

In order to produce high quality maps, some of the measurements weren't retained for the map. The objective function indicates whether the inverse problem was well-posed or ill-posed. In case the minimum is not well defined, the inverse problem is ill-posed and the value of the objective function is elevated. Therefore, a maximum value of the objective function is chosen above which all data will be discarded for the final soil moisture map.

5.1.7 Conversion of dielectric permittivities into soil water content

Topp's equation (eq. 2.5), the polynomial relationship to convert the measured dielectric permittivity into VSWC, is used to retrieve a grid of water content data (m^3/m^3).

5.1.8 Kriging

With the aim of obtaining continuous maps, an ordinary kriging is used to interpolate data on the whole parcel. Kriging is a local prediction technique of the Best Linear Unbiased Predictor (BLUP) [69]. It is a weighed linear combination of the neighbour values of VSWC, based on the information of spatial dependence given by the semi-variogram (see eq. 5.1). The semi-variogram evaluates dissimilarity between data for different distance classes in order to observe the degree of spatial dependence of a variable [70].

$$\theta^* = \sum_{i=1}^{n} \lambda_i \theta_i \tag{5.1}$$

With,
θ^* = Predicted VSWC
λ_i = Weight for θ_i
θ_i = Known values of VSWC

5.1.9 Digital elevation model

In order to create a digital elevation model, 191 aerial photos from a DJI Phantom 4 pro drone are taken at 50 metres above the soil surface. The overlap between the photos is of $\sim$ 70% and the drone flies in automatic mode. The reconstruction of the terrain is done with photogrammetry on Agisoft. The resolution of the model is of 2-3 cm.

5.2 Results

5.2.1 Antenna calibration

On the graphs in figure 5.8, we see two curves, H_i measured from the high altitude and H_i calibration from the different measurements above a body of water. Thee graphs span the bandwidth of interest and each dataset shows the calibration for the amplitude and for the phase. We notice that H_i measured and H_i calibration are similar for the dataset of 15/07,

signifying that the antenna was well calibrated. On the contrary, the 27/03 curves are very different, signifying that the antenna was poorly calibrated (see fig. 5.9).

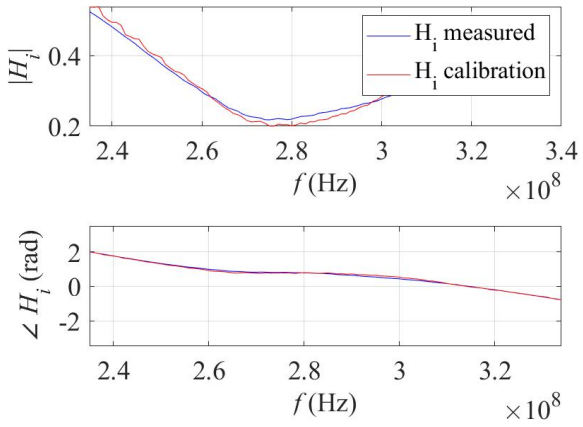

Figure 5.8: Antenna calibration : 15/07.

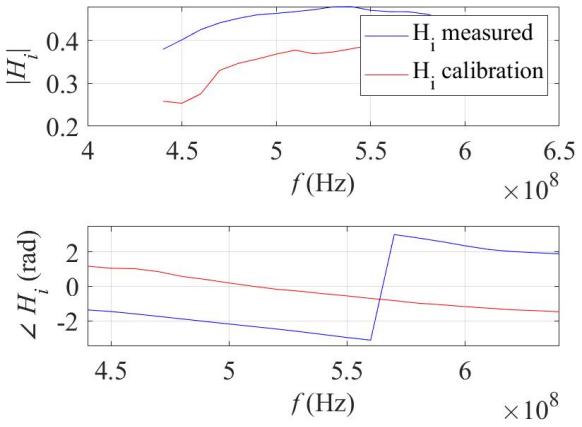

Figure 5.9: Antenna calibration : 27/03.

5.2.2 Radar measurements

For the first dataset (15/07), the measured signal in the time domain is presented on figure 5.10. From this figure, where it is visible that all surface reflections are between 20 and 60 ns, we retrieve the range of altitudes for the LUT. Indeed, since the propagation time is the time for the wave to travel back and forth, when multiplying propagation time by speed of light, we obtain twice the distance between the radar and the soil surface. This signifies that the height of the drone was between 3 and 9 metres during all measurements. This range of altitudes will be used in the LUT for the inversion. The colorbar shows the intensity of the surface reflection S_{11}.

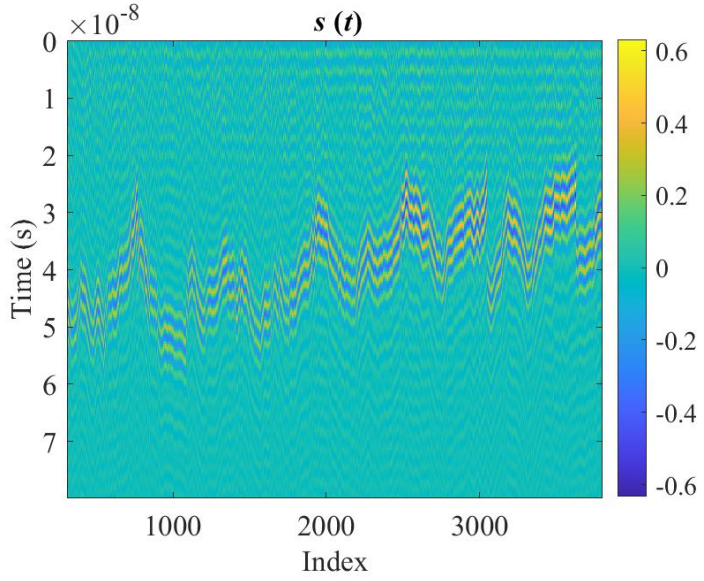

Figure 5.10: Measured signal in the time domain (S_{11}) : 15/07.

For the 27/03 campaign, as visible on fig. 5.11 all surface reflections are between 6 and 40

ns, which results in a choice of altitude range for the LUT between 1 and 6 metres.

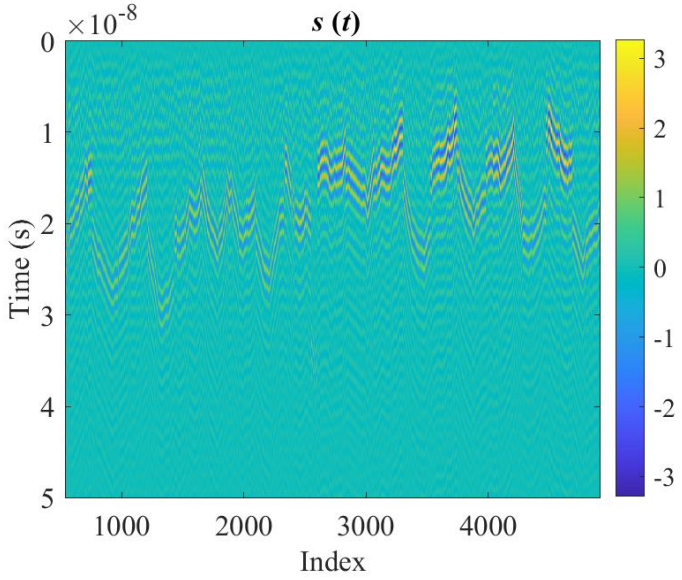

Figure 5.11: Measured signal in the time domain (S_{11}) : 27/03.

5.2.3 Inverted radar signals

For each inverted measurement, two graphs like the one in figure 5.12 and 5.13 are available when running the matlab code. The first figure (fig. 5.12) shows the value of the objective function for the defined ranges of relative permittivies and heights. On the colormap, the bluest region will thus define where the objective function is minimal and where the fit is the best. The second figure (fig. 5.13) shows the fit between the measured and modelled signal when the objective function is minimal. For all measurements in the 15/07 dataset, the model curve fits very well to the measurement curve except at small times. For the 27/03 dataset, the fit is not as good.

Since the quality of the inversion is measured by the objective function, a histogram is used to assess which data points should be discarded (see fig. 5.14 and 5.15). For the 15/07 dataset, the minimum objective functions go from about 0 to 3, but all results for which the objective function is above 2 are discarded. In total, 108 points were discarded (∼4% of all results), which leaves 2652 measurements for the map. For the 27/03 dataset, the minimum objective functions go from about 0 to 80, but all results for which the objective function is above 40 are discarded. In total, 227 points were discarded (∼12% of all results), which leaves 1666 measurements for the map.

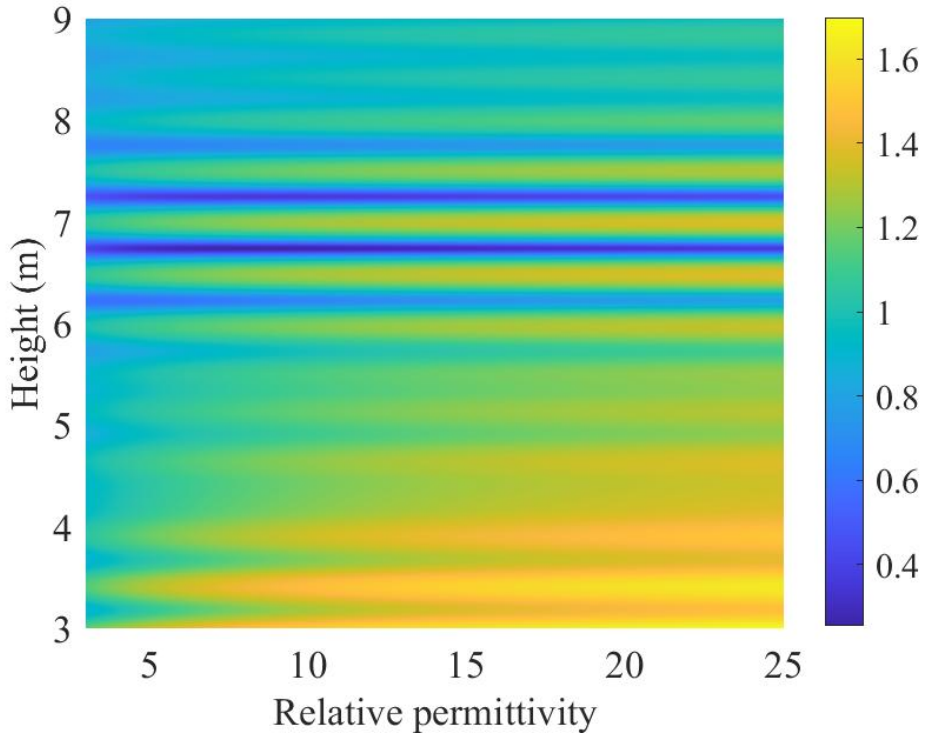

Figure 5.12: Objective function for the whole range of the LUT for one measurement : 15/07.

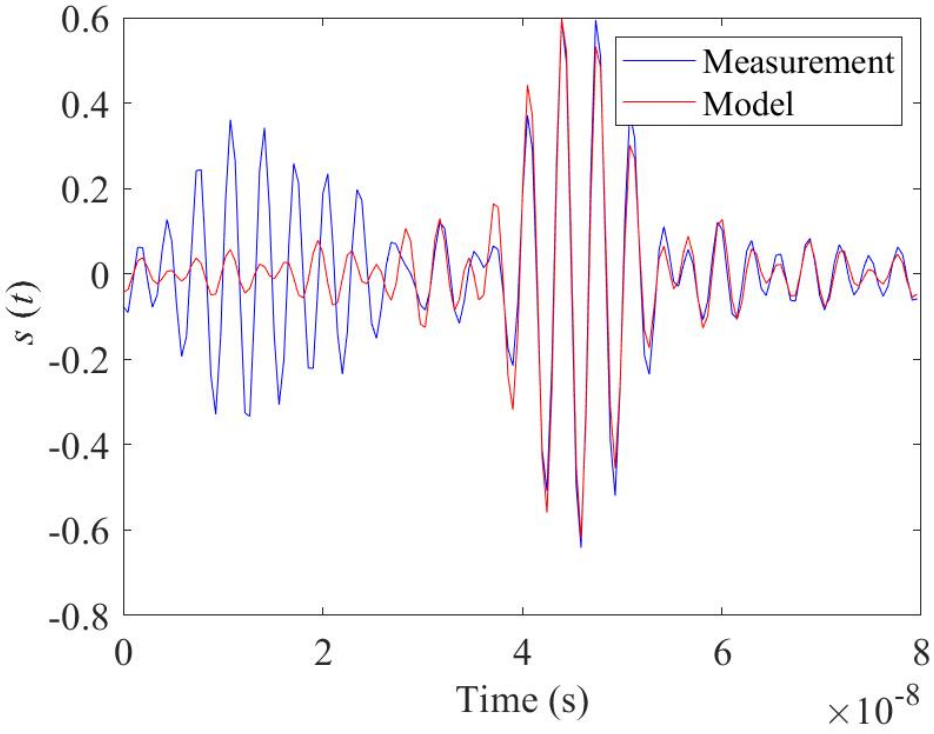

Figure 5.13: Measured and modelled signal in the time domain showing the quality of the fit for one measurement : 15/07.

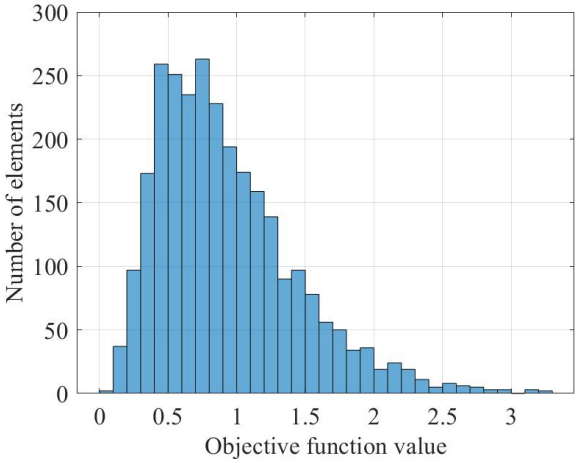

Figure 5.14: Distribution of the objective functions at its minimum value : 15/07.

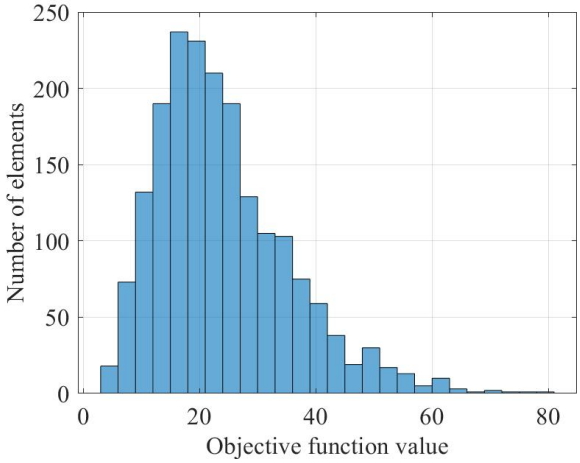

Figure 5.15: Distribution of the objective functions at its minimum value : 27/03.

5.2.4 Soil water content

The distribution of all retained volumetric soil water contents for the first dataset is more or less comprised between 0.05 and 0.3 m^3/m^3 with a mean VSWC of 0.135 m^3/m^3. For the second dataset, the distribution of VSWC is comprised between 0.1 and 0.4 m^3/m^3 with an average value of 0.288 m^3/m^3 (see fig. 5.16 and 5.17).

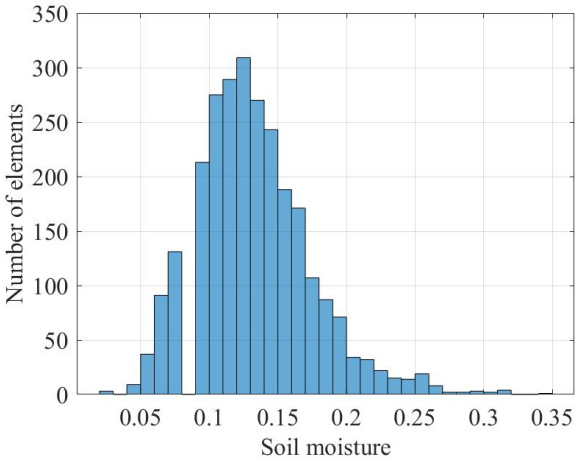

Figure 5.16: Histogram of VSWC on the the field : 15/07.

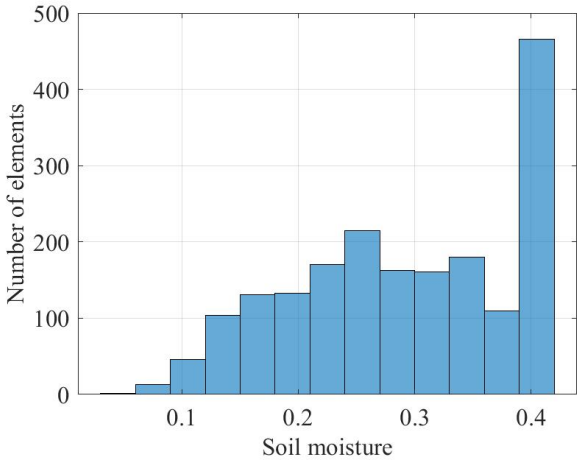

Figure 5.17: Histogram of VSWC on the the field : 27/03.

5.2.5 Kriged maps

The kriged maps were realised using the ordinary kriging module from SAGA in QGIS and are presented on the next page. Both maps use a viridis color scale with low SWC represented by yellow and high SWC values in blue.

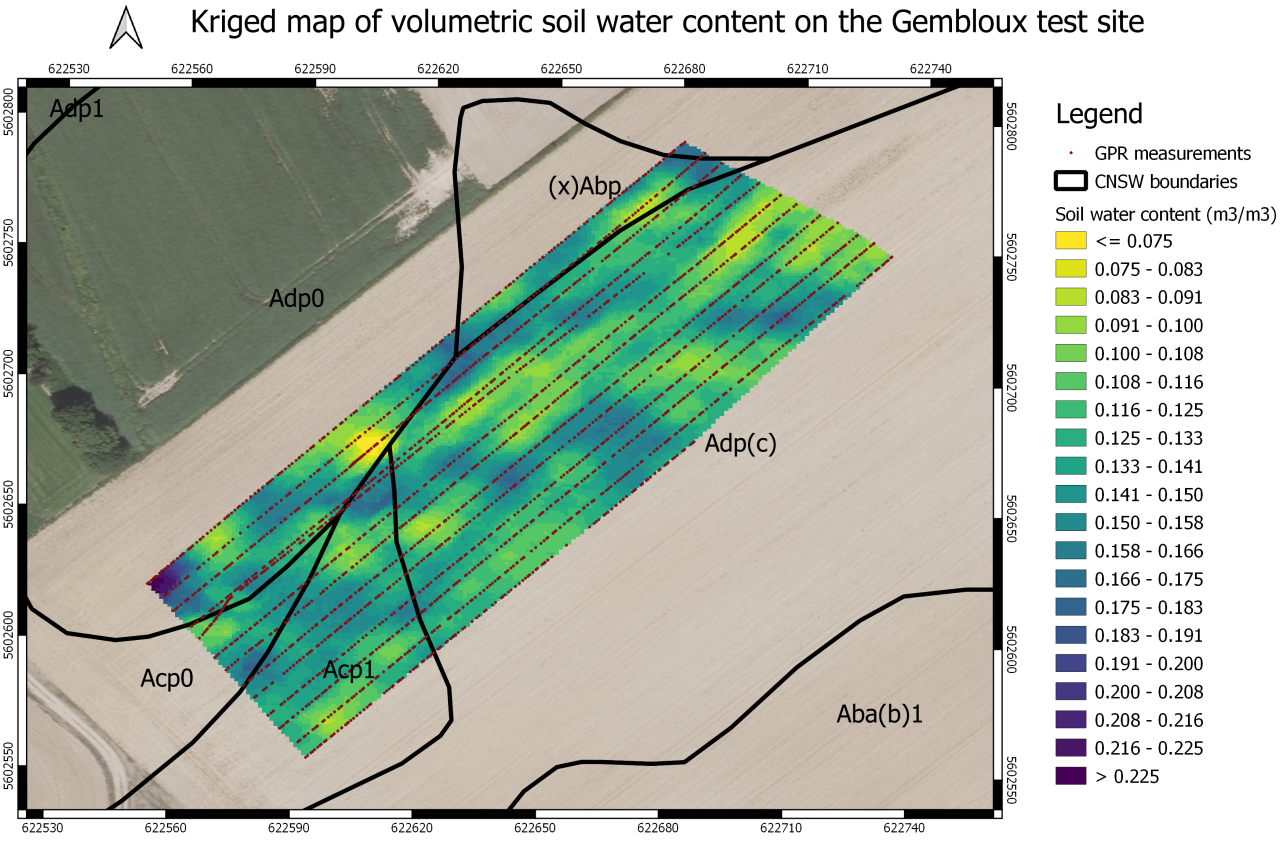

Figure 5.18: Krigged map of the field : 15/07 dataset. Coordinates are in Belgian Lambert 72 (m). WGS84 DATUM.

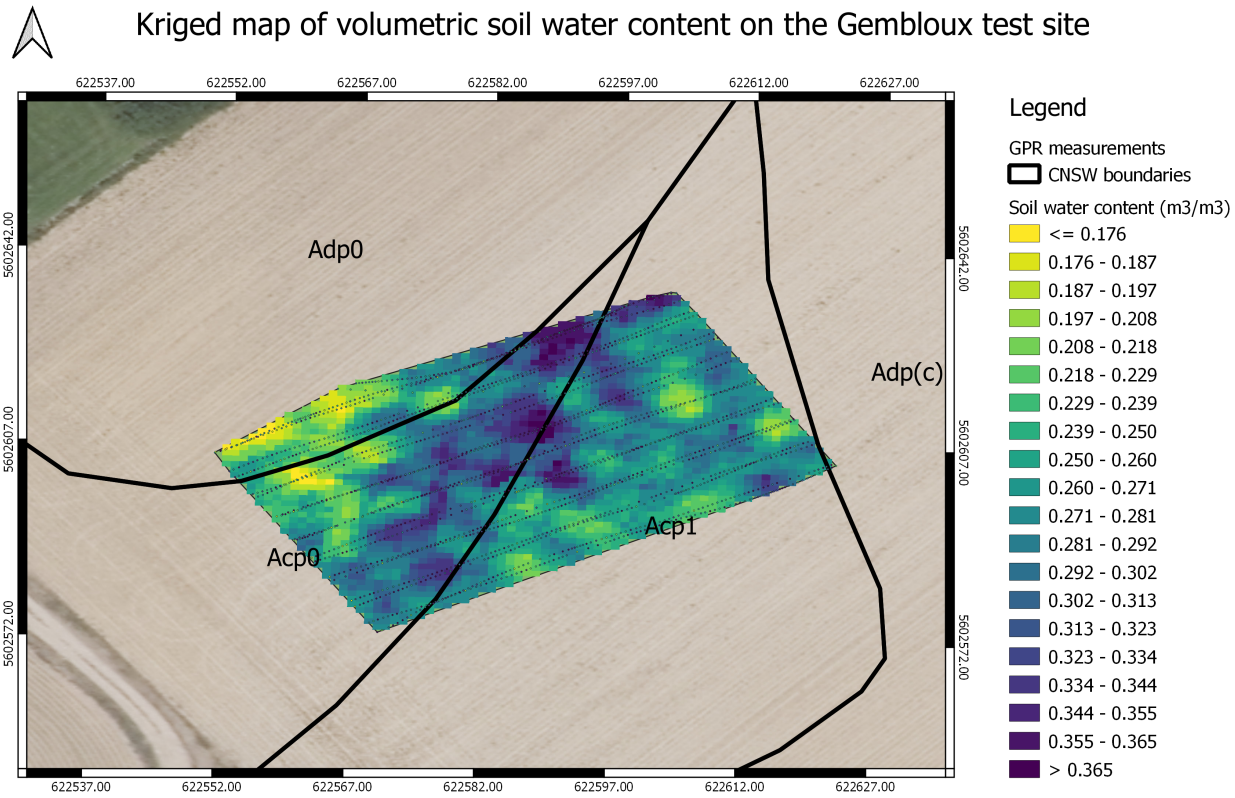

Figure 5.19: Krigged map of the field : 27/03 dataset. Coordinates are in Belgian Lambert 72 (m). WGS84 DATUM.

5.2.6 Digital elevation model

Post processing of aerial images yields the following digital elevation model, cut to fit both kriged areas. There is a clear ascending slope from north to south with 10 metres of difference for the 1.6 ha area.

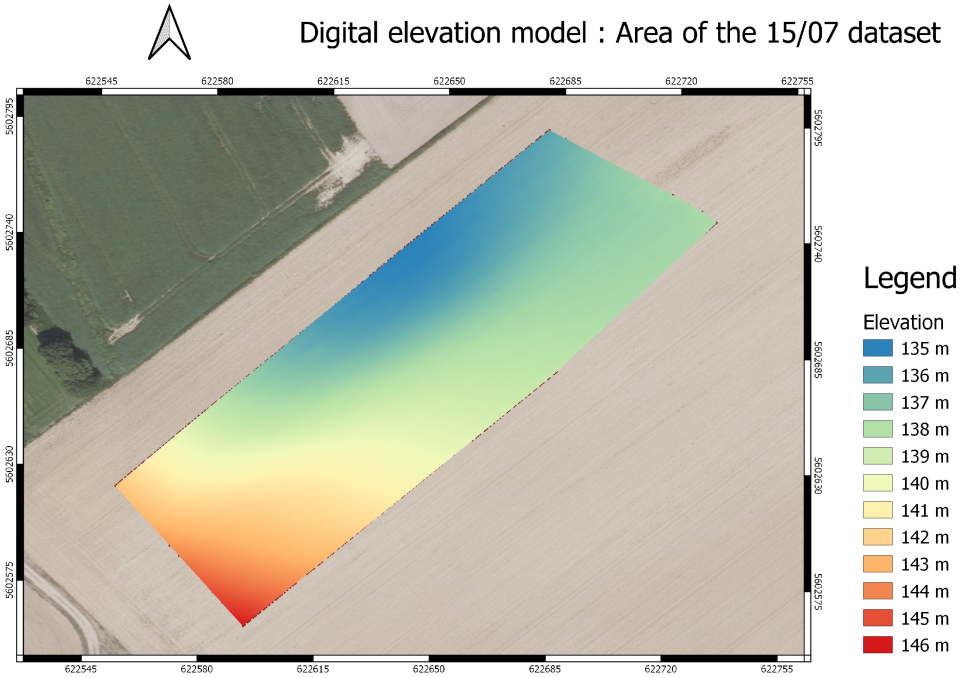

Figure 5.20: Digital elevation model for the area of the first kriged map : 15/07. Coordinates are in Belgian Lambert 72 (m). WGS84 DATUM.

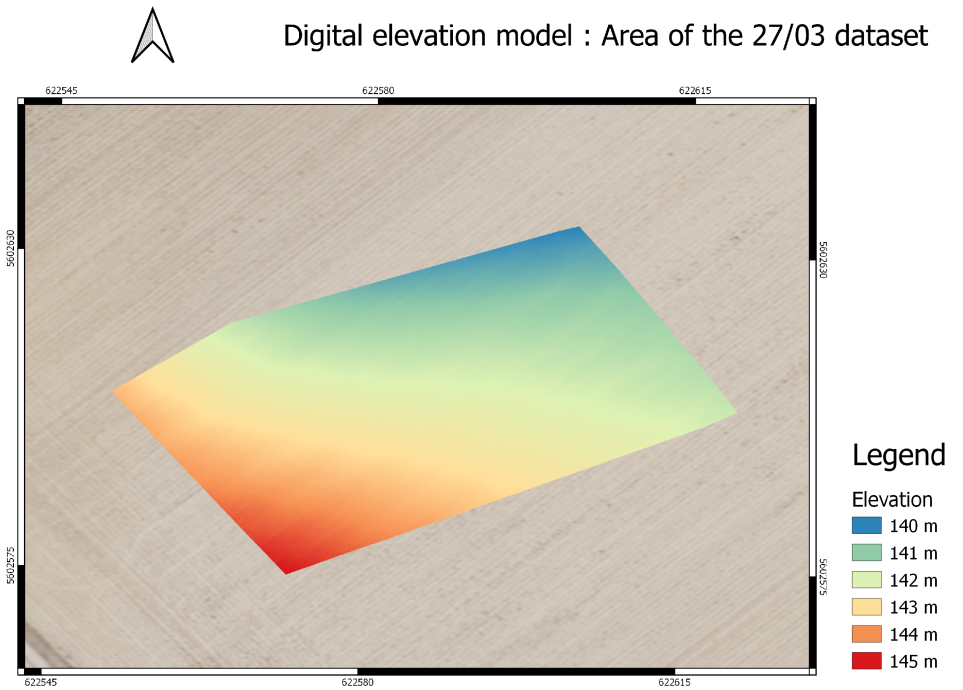

Figure 5.21: Digital elevation model for the area of the second kriged map : 27/03. Coordinates are in Belgian Lambert 72 (m). WGS84 DATUM.

5.3 Discussion

The results for the two flights seem to be quite good. The main flight had a very good calibration of the antenna, but the drone flew quite high which resulted in a poor signal to noise ratio. From far away, the surface reflection is weaker and the amplitude approaches the amplitude of noise. For this reason the fit between the measured and modelled signal seemed to be very good for all measurements for larger times, but not as good for small times. The 27/03 flight had the advantage of being much lower. The surface reflection had a much bigger amplitude which enables a much better signal to noise ratio. This difference in amplitude is also visible on the scales of the colorbar in figures 5.10 and 5.11. However, the 27/03 flight had a very poor antenna calibration, which resulted in unsatisfactory fits.

The soil moisture maps seem relatively consistent with the climate. Indeed, the mean soil moisture was of 0.135 m^3/m^3 for July 15th and of 0.288 m^3/m^3 for March 27th. This corresponds to a wetter soil in March and a dryer soil in June, which is steady with the higher temperatures, rarer precipitations and lower humidity in the first half of July compared with March (see also VSWC histograms in figures 5.16 and 5.17).

	July 15th	**March 27th**
Mean soil moisture	0.135 m^3/m^3	0.288 m^3/m^3
Mean temperature for the month	17°C	6°C
Total monthly precipitations	47.4 mm	81.2 mm
Monthly relative humidity	67%	70%

Table 5.1: Comparison between the two measurement campaigns relatively to the climate

The July map (fig. 5.18) seems to have alternating bands of wetter and dryer soil running horizontally across the field for which no reasonable explanation has been found yet. These horizontal lines are roughly perpendicular to the slope of the field as visible in the DEM (figure 5.20), which could be logical since water accumulates on gentle slopes and runs-off from steep slopes. There is however a considerable probability that this is a coincidence since the digital elevation model seems to be erroneous (see below for discussion about the DEM).

The March map (fig. 5.19) shows a clear central diagonal ridge of wetter soil from south-southwest to north-northeast which coincides roughly with a CNSW boundary. The wetter CNSW class corresponds to Acp0 (moderate drainage, little gleyed) and the neighbour clusters are Adp0 (imperfect drainage, moderately gleyed) and Acp1 (moderate drainage). However the soil moisture map barely overlaps the Adp0 so no interpretation will be made given that soils are continuous. The boundary between both clusters is gradual but modelled by a discontinuity in the CNSW file. Some sense can be found in the observation of the transition between Acp0 and Acp1 since gleyed soils retain water and the gleyed cluster corresponds to the wetter area. There seems to be no correlation between the DEM and the SWC maps for the 27/03 campaign.

The two datasets had different frequency ranges, the July dataset had a lower frequency range (234 - 335 MHz) than the March dataset (440 - 460 MHz). In theory, the lower frequencies (July dataset) can penetrate the soil more in depth, but the resolution isn't as good [71].

Some statistical variables are given in the table below (see table 5.2) and histograms of SWC are available in the results section. Using the standard deviation, it can be concluded that there was less within-field variability for the July dataset. This result is surprising because it contradicts the theory that states that there is more SWC variability on a dryer soil. This theory is based on the fact that there is variability in soil texture and structure which causes variability in water holding capacities [72] [73].

	July 15th	**March 27th**
Mean soil moisture	0.135 m^3/m^3	0.288 m^3/m^3
Standard deviation	0.042 m^3/m^3	0.090 m^3/m^3
Minimum soil moisture	0.030 m^3/m^3	0.043 m^3/m^3
Maximum soil moisture	0.345 m^3/m^3	0.400 m^3/m^3

Table 5.2: Statistical characteristics of both datasets

Unfortunately, the digital elevation model (see fig. 5.20 and 5.21) doesn't appear to be correct. For a reason that is yet to be understood, the values of elevation above sea level seem to be false both relatively and in absolute. Indeed, a GPS reading on the field as well as the WalOnMap interactive map from the Walloon "Géoportail" showed that the field was at 163 - 166 metres instead of 135 - 146 m. While an absolute error is not unusual, it is quite surprising that even the relative accuracy should be wrong.

Chapter 6

Conclusion and prospects

6.1 Conclusion

With a fast growing human population and its ever increasing needs, it is anticipated that global food, fibre, and biofuel demand may double by 2050. To meet this demand, crop production will be obligated to expand up to 140% or more according to estimates by the FAO [20] [74]. Given that freshwater availability will be a limiting factor in reaching this goal sustainably, there will be value in collected data obtained from soil water content monitoring in the framework of precision agriculture. At a time of information technology, collecting and using dense grids of data to inform decision makers in the agricultural sector will be crucial to enhance crop quality and irrigation efficiency and maximise yield, as well as preventing damage from waterlogging and salinisation [25] [38].

Ground penetrating radar has been identified as a promising tool for soil water content monitoring at the field scale. It provides a rapid and off-ground investigation, yielding high resolution, accurate and reproducible maps.

In this thesis, only two measurement campaigns were made. Indeed, due to the Covid19 lockdown, all field and laboratory work was discontinued. On March 27th, my supervisor Pr. Lambot had the opportunity to realise a flight, but unfortunately the antenna calibration was poor, and no access to the lab was given to recalibrate it. When data acquisition was finally possible again, there remained too little time to perfect the automatic flight with constant altitude and for this reason, only one dataset with good antenna calibration was generated but where the flying altitude wasn't quite low enough and wasn't perfectly constant. These two datasets could still be used to produce soil moisture maps and characterise the soil moisture on the field.

Regardless of these conditions, two soil moisture maps were produced and a lot of trial and error will be of use for future research. Unfortunately, no ground-truth validation was possible because of laboratory access restrictions, and no significant validation through correlation with the digital elevation model was found. But on the positive side, this gives place to a good load

of prospects for further drone-borne GPR research. Below is a non-exhaustive list of these prospects for future researchers in the GPRLouvain team.

6.2 Prospects

Future drone-borne GPR for soil moisture mapping will need to perfect the automatic flight system combined with the Lidar, remaining at 2-3 metres of altitude in order to ensure a stable flight with limited changes of incidence angle and an appropriate distance between the soil and the antenna. The optimal soil-antenna distance for which the far field hypothesis is respected but the signal to noise ratio is best should also still be analysed. This study should include safety parameters based on the digital elevation model and the speed of the drone to prevent the drone to crash if slopes are abrupt.

Another interesting prospect is the automation of radar data processing and inversion. Until now, the user has had to actively input parameters during the whole data treatment process. For example, an artificial intelligence that detects minimum and maximum reflection times in the graph of measured signals could determine the altitude ranges for the look-up table and directly use them. Automation would also be useful for selection of free space measurements and the area of interest as well as the kriging of the map on QGIS. Establishing objective criterion for choosing the maximum objective function value below which results are kept would also make it possible to automate the process of exclusion of results for which the inverse problem is ill-posed. In this thesis, a arbitrary value was chosen based on a visual analysis of the histogram. This resulted in 4% of eliminated data for one dataset and 12% in the other.

Future research would benefit from constructing another TEM horn antenna, since these models have better directivity than the dipole. It would also be necessary to restore drone crash security settings to a lower value to prevent accidents.

In this thesis, no validation of results was made. In the future, validation could be made with ground truths, orthophotography, the digital elevation model, a map of intensity of slopes and in-lab texture analysis. On the orthophotography, it would have been nice to compare the color of the wheat with the moisture.

No analysis of the dynamics of soil water content was made in this thesis since there were only two datasets. A time-lapse measurement campaign would make temporal variability analysis possible. A next measurement campaign could also benefit from choosing a field with high CNSW contrasts and/or steep slopes in order to detect significant correlations.

Including soil electrical conductivity data as a validation technique with low frequency GPR, EMI, and/or ERT would be interesting because electrical resistivity is a property that is usually coherent with soil water status [32].

Finally, a market survey and spatial and temporal analysis could be made, determining whether there is a significant within-field variability of SWC that would justify implementing variable rate irrigation, or simply a smart irrigation scheduling.

Bibliography

[1] Environmental protection agency, "Global greenhouse gas emissions data." `https://www.epa.gov/ghgemissions/global-greenhouse-gas-emissions-data`. Accessed: 2020-03-28.

[2] T. Sauer, P. Havlík, U. A. Schneider, E. Schmid, and G. Kindermann, "Agriculture and resource availability in a changing world: The role of irrigation," *Water Resources Research*, vol. 46, 2010.

[3] Sustainable Development Goals Knowledge Platform, "Food security and nutrition and sustainable agriculture." `https://sustainabledevelopment.un.org/topics/foodagriculture`. Accessed: 2020-03-26.

[4] J. Sheffield and E. F. Wood, "Global Trends and Variability in Soil Moisture and Drought Characteristics, 1950–2000, from Observation-Driven Simulations of the Terrestrial Hydrologic Cycle," *Journal of Climate*, vol. 21, pp. 432–458, 02 2008.

[5] T. G. Huntington, "Chapter one - climate warming-induced intensification of the hydrologic cycle: An assessment of the published record and potential impacts on agriculture," vol. 109 of *Advances in Agronomy*, pp. 1 – 53, Academic Press, 2010.

[6] H. Kitabata, K. Nishizawa, Y. Yoshida, and K. Maruyama, "Permafrost thawing in circumarctic and highlands under climatic change scenario projected by community climate system model (ccsm3)," *Sola*, vol. 2, pp. 53–56, 01 2006.

[7] Y. Deng, S. Wang, X. Bai, G. Luo, L. Wu, Y. Cao, H. Li, C. Li, Y. Yang, Z. Hu, and S. Tian, "Variation trend of global soil moisture and its cause analysis," *Ecological Indicators*, vol. 110, p. 105939, 2020.

[8] M. Zhao and S. W. Running, "Drought-induced reduction in global terrestrial net primary production from 2000 through 2009," *Science (American Association for the Advancement of Science)*, vol. 329, no. 5994, pp. 940–943, 2010.

[9] J. K. Green, S. I. Seneviratne, A. M. Berg, K. L. Findell, S. Hagemann, D. M. Lawrence, and P. Gentine, "Large influence of soil moisture on long-term terrestrial carbon uptake," 2019.

[10] E. M. Haacker, V. Sharda, A. M. Cano, R. A. Hrozencik, A. Núñez, Z. Zambreski, S. Nozari, G. E. B. Smith, L. Moore, S. Sharma, P. Gowda, C. Ray, M. Schipanski, and R. Waskom,

"Transition pathways to sustainable agricultural water management: A review of integrated modeling approaches," *JAWRA Journal of the American Water Resources Association*, vol. 55, no. 1, pp. 6–23, 2019.

[11] C. Brouwer, A. Goffeau, and M. Heibloem, *Irrigation Water Management: Training Manual No. 1 - Introduction to Irrigation*. Food and Agriculture Organization of the United Nations, Rome, 1985. Accessed: 2020-04-15.

[12] J. Bruinsma, *World Agriculture: Towards 2015/2030 – An FAO Perspective*. Food and Agriculture Organization of the United Nation, Rome, 2003.

[13] T. Oki and S. Kanae, "Global hydrological cycles and world water resources," *Science*, vol. 313, no. 5790, pp. 1068–1072, 2006.

[14] P. Waller and M. Yitayew, *Irrigation and Drainage Engineering*. Cham: Springer International Publishing AG, 1st ed., 2016;.

[15] W. R. Walker, *Guidelines for Designing and Evaluating Surface Irrigation Systems*. Food and Agriculture Organization of the United Nations, Rome, 1989.

[16] C. Brouwer, K. Prins, M. Kay, and M. Heibloem, *Irrigation Water Management: Irrigation Methods*. Food and Agriculture Organization of the United Nations, Rome, 1989.

[17] D. Hillel, *Small-scale irrigation for arid zones*. Food and Agriculture Organization of the United Nations, Rome, 1997. Accessed: 2020-04-15.

[18] Food and Agriculture Organisation of the United Nations, *Agriculture Water Management*. Accessed: 2020-04-08.

[19] D. Hillel, A. K. Braimoh, and P. L. G. Vlek, *Soil Degradation Under Irrigation*, pp. 101–119. Dordrecht: Springer Netherlands, 2008.

[20] Q. Chai, Y. Gan, N. C. Turner, R.-Z. Zhang, C. Yang, Y. Niu, and K. H. Siddique, "Water-saving innovations in chinese agriculture," vol. 126 of *Advances in Agronomy*, pp. 149 – 201, Academic Press, 2014.

[21] P. Alexander, S. Rabin, P. Anthoni, R. Henry, T. A. M. Pugh, M. D. A. Rounsevell, and A. Arneth, "Adaptation of global land use and management intensity to changes in climate and atmospheric carbon dioxide," *Global Change Biology*, vol. 24, no. 7, pp. 2791–2809, 2018.

[22] A. Utset and M. Borroto, "A modeling-gis approach for assessing irrigation effects on soil salinisation under global warming conditions," *Agricultural Water Management*, vol. 50, no. 1, pp. 53 – 63, 2001.

[23] A. Ghatak, P. Chaturvedi, and W. Weckwerth, "Cereal crop proteomics: Systemic analysis of crop drought stress responses towards marker-assisted selection breeding," *Frontiers in Plant Science*, vol. 8, p. 757, 2017.

[24] N. Zhang, M. Wang, and N. Wang, "Precision agriculture—a worldwide overview," *Computers and Electronics in Agriculture*, vol. 36, no. 2, pp. 113 – 132, 2002.

[25] N. R. Council, *Precision Agriculture in the 21st Century: Geospatial and Information Technologies in Crop Management*. Washington, DC: The National Academies Press, 1997.

[26] N. M. Cid-Garcia, V. Albornoz, Y. A. Rios-Solis, and R. Ortega, "Rectangular shape management zone delineation using integer linear programming," *Computers and Electronics in Agriculture*, vol. 93, pp. 1 – 9, 2013.

[27] A. Haghverdi, B. G. Leib, R. A. Washington-Allen, P. D. Ayers, and M. J. Buschermohle, "Perspectives on delineating management zones for variable rate irrigation," *Computers and Electronics in Agriculture*, vol. 117, pp. 154 – 167, 2015.

[28] W. R. Mendes, F. M. U. Araújo, R. Dutta, and D. M. Heeren, "Fuzzy control system for variable rate irrigation using remote sensing," *Expert Systems With Applications*, vol. 124, pp. 13–24, 2019.

[29] X. Shi, W. Han, T. Zhao, and J. Tang, "Decision support system for variable rate irrigation based on uav multispectral remote sensing," *Sensors (Basel, Switzerland)*, vol. 19, no. 13, p. 2880, 2019.

[30] The Community Research and Development Information Service, "Waterbee smart irrigation systems demonstration actions." `https://cordis.europa.eu/project/id/283638`, 2016.

[31] I. Lunt, S. Hubbard, and Y. Rubin, "Soil moisture content estimation using ground-penetrating radar reflection data," *Journal of Hydrology*, vol. 307, no. 1, pp. 254 – 269, 2005.

[32] F. Andre, C. van Leeuwen, S. Saussez, R. Durmen, P. Bogaert, D. Moghadas, L. Rességuier, B. Delvaux, H. Vereecken, and S. Lambot, "High-resolution imaging of a vineyard in south of france using ground-penetrating radar, electromagnetic induction and electrical resistivity tomography," *Journal of Applied Geophysics*, vol. 78, pp. 113–122, 03 2012.

[33] C. M. Steelman and A. L. Endres, "Comparison of petrophysical relationships for soil moisture estimation using gpr ground waves," *Vadose Zone Journal*, vol. 10, no. 1, pp. 270–285, 2011.

[34] A. Robock, "Hydrology, floods and droughts : Soil moisture," in *Encyclopedia of Atmospheric Sciences* (G. R. North, J. Pyle, and F. Zhang, eds.), pp. 232 – 239, Oxford: Academic Press, 2nd ed., 2015.

[35] M. Kirkham, "Chapter 9 - dual thermal probes," in *Principles of Soil and Plant Water Relations (Second Edition)* (M. Kirkham, ed.), pp. 123 – 151, Boston: Academic Press, second edition ed., 2014.

[36] G. C. Topp, J. L. Davis, and A. P. Annan, "Electromagnetic determination of soil water content: measurements in coaxial transmission lines," *Water Resources Research*, vol. 16, no. 3, pp. 574–582, 1980.

[37] J. A. Huisman, S. S. Hubbard, J. D. Redman, and P. A. Annan, "Measuring soil water content with ground penetrating radar: a review," *Vadose Zone Journal*, vol. 2, pp. 476–491, 2003.

[38] K. Grote, S. Hubbard, and Y. Rubin, "Field-scale estimation of volumetric water content using ground-penetrating radar ground wave techniques," *Water Resources Research*, vol. 39, no. 11, 2003.

[39] H. M. Jol, *Ground Penetrating Radar Theory and Applications*. NL: Elsevier Science, 2009;2008;.

[40] A. P. Annan, *Chapter 1 - Electromagnetic Principles of Ground Penetrating Radar*, pp. 1–40. Elsevier Science & Technology.

[41] L. Slater and X. Comas, "Chapter 7 - the contribution of ground penetrating radar to water resource research," in *Ground Penetrating Radar Theory and Applications* (H. M. Jol, ed.), pp. 203 – 246, Amsterdam: Elsevier, 2009.

[42] L. W. Galagedara, G. W. Parkin, and J. D. Redman, "An analysis of the ground-penetrating radar direct ground wave method for soil water content measurement," *Hydrological Processes*, vol. 17, no. 18, pp. 3615–3628, 2003.

[43] Q. Cao, X. Song, H. Wu, L. Gao, F. Liu, S. Yang, and G. Zhang, "Mapping the response of volumetric soil water content to an intense rainfall event at the field scale using gpr," *Journal of Hydrology*, vol. 583, p. 124605, 2020.

[44] S. Lambot, L. Weihermüller, J. A. Huisman, H. Vereecken, M. Vanclooster, and E. C. Slob, "Analysis of air-launched ground-penetrating radar techniques to measure the soil surface water content," *Water Resources Research*, vol. 42, no. 11, pp. W11403–n/a, 2006.

[45] D. Daniels, *Antennas*. 2009.

[46] J. W. Baars, *Antenna characteristics in practical applications*, pp. 55–108. New York, NY: Springer New York, 2007.

[47] N. Fortino, J.-Y. Dauvignac, and G. Kossiavas, "Overview of uwb antennas," 2013.

[48] K. Wu, G. A. Rodriguez, M. Zajc, E. Jacquemin, M. Clément, A. De Coster, and S. Lambot, "A new drone-borne gpr for soil moisture mapping," *Remote Sensing of Environment*, 2019.

[49] S. Lambot, *Hydrogeophysical characterization of soil using ground penetrating radar*. PhD thesis, 2003.

[50] J. Ježová and S. Lambot, "A dielectric horn antenna and lightweight radar system for material inspection," *Journal of Applied Geophysics*, vol. 170, p. 103822, 2019.

[51] A. R. Mallahzadeh and F. Karshenas, "Modified tem horn antenna for broadband applications," *Progress In Electromagnetics Research*, vol. 90, pp. 105–119, 01 2009.

[52] W. Ciciora, J. Farmer, D. Large, and M. Adams, "Chapter 7 - signal reception," in *Modern Cable Television Technology (Second Edition)* (W. Ciciora, J. Farmer, D. Large, and M. Adams, eds.), The Morgan Kaufmann Series in Networking, pp. 287 – 332, San Francisco: Morgan Kaufmann, second edition ed., 2004.

[53] S. Farahani, "Chapter 5 - rf propagation, antennas, and regulatory requirements," in *ZigBee Wireless Networks and Transceivers* (S. Farahani, ed.), pp. 171 – 206, Burlington: Newnes, 2008.

[54] S. Lambot, E. C. Slob, I. van den Bosch, B. Stockbroeckx, and M. Vanclooster, "Modeling of ground-penetrating radar for accurate characterization of subsurface electric properties," *IEEE Transactions on Geoscience and Remote Sensing*, vol. 42, no. 11, pp. 2555–2568, 2004.

[55] S. Lambot and F. André, "Full-wave modeling of near-field radar data for planar layered media reconstruction," *IEEE Transactions on Geoscience and Remote Sensing*, vol. 52, no. 5, pp. 2295–2303, 2014.

[56] E. Jacquemin, S. Lambot, and X. Draye, "Analyse de la cartographie de l'humidité de la zone racinaire par géoradar aéroporté basses fréquences," Master's thesis, UCLouvain, 2017.

[57] Emlid Ltd, "Emlid docs." `https://emlid.com/docs/`, 2020. Accessed: 2020-03-22.

[58] European Global Navigation Satellite Systems Agency, *What is GNSS?*, 2020.

[59] O. Heirich, P. Robertson, C. Garcia, T. Strang, and A. Lehner, "Probabilistic localization method for trains," pp. 482–487, 06 2012.

[60] U.S. Department of Transportation : Federal Aviation Administration, "Satellite navigation — ground based augmentation system (gbas)." `https://www.faa.gov/about/office_org/headquarters_offices/ato/service_units/techops/navservices/gnss/laas/`, 2018.

[61] M. Magno, S. Rickli, J. Quack, O. Brunecker, and L. Benini, "Poster abstract: Combining lora and rtk to achieve a high precision self-sustaining geo-localization system," pp. 160–161, IEEE, 2018.

[62] B. Hofmann-Wellenhof, H. Lichtenegger, and E. Wasle, *GNSS - Global Navigation Satellite Systems: GPS, GLONASS, Galileo, and More*. Vienna: Springer Wien, 2007;2008;.

[63] H. Zhang, E. Aldana-Jague, F. Clapuyt, F. Wilken, V. Vanacker, and K. Van Oost, "Evaluating the potential of post-processing kinematic (ppk) georeferencing for uav-based structure-from-motion (sfm) photogrammetry and surface change detection," *Earth Surface Dynamics*, vol. 7, no. 3, pp. 807–827, 2019.

[64] Semtech, "What is lora ?." https://www.semtech.com/lora/what-is-lora, 2020.

[65] P. Seneviratne, *Beginning LoRa Radio Networks with Arduino: Build Long Range, Low Power Wireless IoT Networks*. Berkeley: Apress, 1st ed., 2019.

[66] Sciencing, "What is the difference between rtk fix and rtk float?." https://sciencing.com/difference-between-rtk-fix-rtk-float-12245568.html, 2020.

[67] D. S. M. Valente, A. Momin, T. Grift, and A. Hansen, "Accuracy and precision evaluation of two low-cost rtk global navigation satellite systems," *Computers and Electronics in Agriculture*, vol. 168, p. 105142, 2020.

[68] S. Lambot, M. Antoine, M. Vanclooster, and E. Slob, "Effect of soil roughness on the inversion of off-ground monostatic gpr signal for noninvasive quantification of soil properties," *Water Resources Research, 42, 2006 ; doi:10.1029/2005WR004416*, vol. 42, 03 2006.

[69] S. Y. Chung, S. Venkatramanan, H. E. Elzain, S. Selvam, and M. Prasanna, "Chapter 4 - supplement of missing data in groundwater-level variations of peak type using geostatistical methods," in *GIS and Geostatistical Techniques for Groundwater Science* (S. Venkatramanan, M. V. Prasanna, and S. Y. Chung, eds.), pp. 33 – 41, Elsevier, 2019.

[70] M. D. Nathan Bemelmans, Lucas Limbourg, "Analyse des données spatiales d'une parcelle agricole." Report for LBIRE2101, june 2019.

[71] R. L. Van Dam and W. Schlager, "Identifying causes of ground-penetrating radar reflections using time-domain reflectometry and sedimentological analyses," *Sedimentology*, vol. 47, no. 2, pp. 435–449, 2000.

[72] L. Longchamps, R. Khosla, R. Reich, and D. W. Gui, "Spatial and temporal variability of soil water content in leveled fields," *Soil Science Society of America Journal*, vol. 79, no. 5, pp. 1446–1454, 2015.

[73] F. Hupet and M. Vanclooster, "Intraseasonal dynamics of soil moisture variability within a small agricultural maize cropped field," *Journal of Hydrology*, vol. 261, no. 1, pp. 86–101, 2002.

[74] FAO, *The state of food and agriculture. Climate change, agriculture and food security*. Food and Agriculture Organization of the United Nations, 2016.

Soil moisture mapping using a drone-borne Ground Penetrating Radar

A tool for precision agriculture and soil hydrodynamic modelling

Margot Dehem

Today, the leading consumer of freshwater is agriculture, and it is consuming up to 70% of the extracted volume. Considering a predicted population increase of 30% by 2050 along with a 70% increase in food production, a major challenge for the coming decades will be to innovate and find smart solutions to sustainably manage water consumption for agriculture.

With that in mind, a drone-borne Ground Penetrating Radar (GPR) designed to produce high resolution soil moisture maps is in development in the GPRLouvain research center. This tool is meant to rapidly provide soil water content data and could be used in precision agriculture or variable rate irrigation once it is finalised.

This Covid19-impregnated thesis was not able to treat high volumes of soil moisture data in order to analyse spatial and temporal variability, but it provides a wide bibliographical review of the technology and presents the method and results for the two measurement campaigns. The results seemed quite consistent and serve as proof that there is a bright future for excellent results in soil water content monitoring using drone-borne GPR.

UNIVERSITÉ CATHOLIQUE DE LOUVAIN

Faculté des bioingénieurs

Croix du Sud, 2 bte L7.05.01, 1348 Louvain-La-Neuve, Belgique | www.uclouvain.be/agro